DOE/PC/94066--T6

Isobutanol-Methanol Mixtures from Synthesis Gas

Quarterly Technical Progress Report

Period Covered: 1 January to 31 March 1996

Contractor

University of California-Berkeley
Berkeley, California 94720

Enrique Iglesia - Program Manager

20 April 1996

Prepared for the United States Department of Energy *
Under Contract Number DE-AC22-94PC94066
Contract Period 1 October 1994 - 30 September 1997

RESTRICTED DOCUMENT

This report was produced under Contract No. DE-AC22-94PC94066 for the United States Department of Energy. No portion may be released or published without the written authorization of the contractor and the Department of Energy. U. S. Department of Energy Patent Clearance is not required prior to publication of this document.

---

* This report was prepared as an account of work sponsored by the United States Government. Neither the United States Government nor the United States Department of Energy, nor any of their employees, make any warranty, express or implied, or assumes any legal liability or responsibility for the accuracy, completeness, or usefulness of any information, apparatus, product, or process disclosed, or represents that its use would not infringe privately owned rights. Reference herein to any specific commercial product, process, or service by trade name, trademark, manufacturer, or otherwise does not necessarily constitute or imply its endorsement, recommendation, or favoring by the United States Government or any agency thereof. The views and opinions of authors expressed herein do not necessarily state or reflect those of the United State Government or any agency thereof.

TABLE OF CONTENTS

EXECUTIVE SUMMARY

1. CONTRACT OBJECTIVES AND TASKS

2. SUMMARY OF ACTIVITIES

3. STATUS, ACCOMPLISHMENTS, AND RESULTS

Task 1: Project Work Plan

Task 2: Catalyst Synthesis

Task 3: Catalyst Evaluation in Laboratory Scale Reactors

3.1 Kinetic Studies of Alcohol Coupling Reactions

3.2 Isobutanol Synthesis at High Pressure in the CMRU

Task 4: Identification of Reaction Intermediates

4.1 Determination of Copper Surface Area
4.2 TPSR of Methanol, Ethanol and Acetaldehyde on $Cu/MgO/CeO_2$ Catalysts

Task 5: Bench-Scale Catalyst Evaluation at Air Products and Chemicals

4. PARTICIPATING PROJECT PERSONNEL

5. FIGURES

EXECUTIVE SUMMARY

A series of $CuMgCeO_x$ catalysts have been prepared by coprecipitating the corresponding metal nitrates with a mixed solution of potassium carbonate and potassium hydroxide. The bulk composition of the catalyst has been measured by atomic absorption (AA) analysis and the phase composition has been determined by XRD. The range of copper dispersion (determined by N_2O titration) in these samples (19-48%) are among the highest reported in the literature for Cu-based methanol and higher alcohol synthesis catalysts.

Kinetic studies of methanol and ethanol coupling reactions on Cu/ZnO and K-$Cu/MgO/CeO_2$ catalysts indicate that copper promotes alcohol dehydrogenation. Acetaldehyde is a reactive intermediate, for which self-condensation reactions lead to the formation of acetone, n-butyraldehyde, methyl ethyl ketone (MEK) and ethyl acetate.

High-pressure isobutanol synthesis studies have been carried out on K- and Cs-promoted $Cu/MgO/CeO_2$ catalysts. At 321 °C and 750 psi, 1 wt % K-$Cu_{0.5}Mg_5CeO_x$ gives a CO conversion level of 21 % with methanol isobutanol selectivities of 65 % and 13 %, respectively. Operation at higher temperatures results in decreased conversions with increased selectivities to isobutanol and CO_2. K-promoted $Cu/MgO/CeO_2$ is 2-3 times more active than Cs-promoted $Cu/MgO/CeO_2$ with respect to CO conversion; however, the Cs-promoted catalyst activates the C_1 to C_2 step more effectively as evidenced by a factor of three higher methanol conversion to ethanol. Runs for which low conversions are obtained use catalysts containing too high an alkali loading, as suggested by resultant total and copper surface areas.

Temperature programmed surface reaction (TPSR) studies of methanol, ethanol and acetaldehyde on MgO/CeO_2-based copper catalysts show the evolution of acetone, crotonaldehyde, methyl ethyl ketone, H_2, carbon oxides. They evolved at different temperatures, ranging from 90 °C to 400 °C. Crotonaldehyde, a precursor of n-butanol, comes from the aldol-condensation of acetaldehyde. Both copper metal and reducible metal oxides such as CeO_2 are necessary for the production of acetone (a precursor to 2-propanol). The addition of CO decreases the rate of acetone production, while H_2 increases because of the formation and consumption of CO_2 via water-gas shift reaction. CO_2, a weak acid, blocks the basic sites responsible for higher oxygenates formation. Neither ethanol nor acetaldehyde produces propionaldehyde or 1-propanol, precursors to isobutyraldehyde, suggesting these C_3 species can only form via reactions involving C_1 and C_2 oxygenate species.

1. CONTRACT OBJECTIVES AND TASKS

The contract objectives are:

1. To design a catalytic material for the synthesis of isobutanol with a productivity of 200 g isoalcohols/g-cat-h and a molar isobutanol-to-methanol ratio near unity

2. To develop structure-function rules for the design of catalysts for the selective conversion of synthesis gas to isoalcohols

The research program has been grouped into five specific tasks and a set of project management and reporting activities. The abbreviated designations for these tasks are:

- Project Work Plan ***(Task 1)***

- Catalyst Synthesis ***(Task 2)***

- Catalyst Evaluation in Laboratory Scale Reactors ***(Task 3)***

- Identification of Reaction Intermediates ***(Task 4)***

- Bench-Scale Catalyst Evaluation at Air Products and Chemicals ***(Task 5)***

2. SUMMARY OF ACTIVITIES

Activities during this period have focused on:

- Preparation of a series of K-promoted $Cu/MgO/CeO_2$ catalysts

- Study of methanol and ethanol coupling reactions on ZnO- and MgO/CeO_2-based copper catalysts

- Evaluation of high-pressure isobutanol synthesis reactions using K-$Cu/MgO/CeO_2$ catalysts

- TPSR studies of methanol, ethanol and acetaldehyde on MgO/CeO_2, $Cu/MgO/CeO_2$ and $K\text{-}Cu/MgO/CeO_2$

3. STATUS, ACCOMPLISHMENTS, AND RESULTS

Task 1: Management Plan

No activities were carried out during this reporting period.

Task 2: Catalyst synthesis

Samples were prepared by coprecipitation of 1 M mixed metal nitrate solutions with a mixed solution of potassium hydroxide (2M) and potassium carbonate (1M) at T = 65°C and a constant pH = 9 in a stirred batch reactor using vigorous agitation. The precipitates were filtered, washed with distilled water at 60°C, and then dried at 80-90°C overnight. The resulting materials were calcined at 450°C for 4 h to obtain the mixed oxides. The detailed procedures were described by Apesteguia et al. [1]. Alkali promoted $Cu/MgO/CeO_2$ and its individual components Cu/MgO, MgO/CeO_2, MgO and CeO_2 were prepared; their properties are summarized in Table 1.

BET surface areas (S_g) were measured by nitrogen adsorption at 77 K. The bulk composition of the sample was determined by atomic absorption (AA) spectroscopy. The atomic ratios of Mg/Cu and Mg/Ce are in good agreement with the theoretical values. Irreproducibility in K-loading (0.4 - 3.5 wt %) of $Cu/MgO/CeO_2$ and Cu/MgO has resulted even though the samples have been thoroughly washed. The amount of potassium left on MgO/CeO_2 is even greater. The unusually low surface area of MG3-1O/K ($K-Cu/MgO/CeO_2$) was attributed to the presence of large amount of potassium on the catalyst.

Table 1. Composition and surface area of the catalytic oxides

Sample	Mg/Cu	Mg/Ce	K, wt.% (nominal)	K, wt.% (AAS)	Sg (m^2/g)	Cu Dispersion,%
MG3 - 1 O	9.4	3.9	< 0.01	4.1	62	
MG3 - 1 O/K	10.4	5.7	3.0	6.5	32	
MG3 - 1b O			< 0.01	0.4	108	48
MG3 - 1b O/K	8.6	4.7	1.0	1.5	88	19
MG3 - 10 O	9.6	4.7	< 0.01		96	
MG3 - 10 O/K			1.0		190	
MG3 - 10 O/Cs			3.4		143	
MG3 - 10 bO/K	11.1	4.8	1.0	1.0	162	23
MG3 - 11 O			< 0.01	2.6	93	
MG3 - 11 O/K			1.0	3.5		
MG3 - 2 (Mg-Ce)	-----	4.6	<0.01	5.3	53	
MG3 - 3 (Ce)		-----			0.2	
MG3 - 4 (Mg)	-----	-----			1.5	
MG3 - 5 (Cu-Mg)	8.0	-----	<0.01	0.2	118.0	

A typical powder X-ray diffraction (XRD) spectrum of the Cu-Mg-Ce precursor is shown in Fig. 1. $Mg(OH)_2$ (brucite) and $Ce(OH)_3$ were identified while $Cu(OH)_2$ or carbonates were not detected. During the calcination of a Cu-Mg-Ce precursors, a typical weight loss of about 22-23% was observed. Based on the nominal composition and the phases detected by XRD (Fig. 1), the experimental total weight loss upon calcination is very close to the predicted one (~23.5%).

The phase compositions of $Cu/MgO/CeO_2$, MgO/CeO_2, MgO and CeO_2 calcined at 450 °C were determined by XRD and the results are shown in Figure 2. The MG3-1 O ($Cu/MgO/CeO_2$) sample (Fig. 2a) showed two phases: CeO_2 (cerianita) and MgO (periclase). The CuO phase was not detected, suggesting that copper oxide was well dispersed or formed a solid solution upon Cu^{2+} insertion into the ceria lattice [2]. Lamonier et al. [2] have found that for a wide range of cerium/copper compositions, a solid solution is always formed by insertion of Cu^{2+} ions in substitutional positions in the ceria lattice. This process occurs at the coprecipitation step and is maintained during calcination. The Cu-free MG3-2 O sample (Fig. 2b) showed the same phases as MG3-1 O. The MG3-3 O sample gave only a phase attributed to CeO_2 (Fig. 2c). For MG3-4 O sample which is a magnesium oxide, a MgO periclase phase as well as an unknown phase were observed (Fig. 2d). The unknown phase might be related to the potassium compounds left on the surface.

For catalysts with approximately equal compositions, the surface areas shown in Table 1 vary from sample to sample. This is a result of different amount of potassium left in the catalyst after precipitation. The presence of potassium might cause the sintering of the catalyst. It is noteworthy that the surface area of MG3-10 O/K is twice as much as that of MG3-10 O though the amount of potassium is expected to be larger in the former. This is interpreted by the fact that MG3-10 O/K was prepared via incipient wetness of MG3-10 O using K_2CO_3 solution. During this process, MG3-10 O was re-exposed to water where MgO was converted back to hydroxide, resulting in a higher surface area after calcination. It has been well established that the commercial, low surface area MgO (15-30 m^2/g) can be readily transformed to high surface area MgO (100-300 m^2/g) by hydrating MgO in boiling water and then calcining at temperatures > 400 °C [3-5]. Neither MgO nor CeO_2 gave a surface area greater than 1 m^2/g in this work. The low surface area could be attributed to the presence of residual potassium ions left during catalyst preparation. As reported by Lunsford and co-workers [6,7], the addition of lithium to MgO resulted in a marked decrease in MgO surface area due to sintering.

Both MG3-10 O/K and MG3-10 bO/K were prepared from MG3-10 O, but via different pathways. In the case of MG3-10 O/K, the precursor was calcined at 450 °C prior to potassium impregnation. After impregnation, the sample was recalcined at 450 °C for 4 h, and the resulting material was designated as MG-10 O/K. MG3-10 bO/K was prepared by impregnating the precursor with potassium carbonate before subject to calcination at 450 °C.

The XRD spectra of MG3-10 bO and MG3-10bO/K are shown in Fig. 3a and 3b. No significant difference in crystallinity between these two samples was observed. Only CeO_2 and MgO phases were present. The low signal-to-noise ratio indicates that these samples were amorphous.

Task 3: Catalyst Evaluation in Laboratory Scale Reactors

3.1 Kinetic Studies of Alcohol Coupling Reactions

Alcohol coupling reactions consist of a sequence of steps leading to the formation of higher alcohols from C_1 and C_2 alcohols [8,9]. These steps include alcohol dehydrogenation to aldehydes, aldol condensation of aldehydes to higher oxygenates, and the subsequent hydrogenation to higher alcohols. It is believed that aldehydes are the reactive intermediates in chain growth [10]. The aldol condensation reaction occurs on either acidic or basic catalyst in the presence of aldehydes or ketones with α-hydrogen [11].

In a typical experiment, 22 mg of catalyst was charged into a gradientless batch reactor. The sample was reduced in 10 % H_2 in He at 350 °C for 30 min. After the desired reaction temperature was achieved, a reaction mixture was introduced into the reactor. For the coupling reaction with methanol and ethanol on Cu/ZnO (30/70 at.%), the following gas composition was used: ethanol/methanol/Ne/He = 30/60/15/655 Torr. Neon was used as an internal standard. In ethanol dehydrogenation experiments, the ethanol partial pressure was 30 Torr with the balance helium. The reaction was carried out at 760 Torr in a recirculating reactor unit (RRU). Products were sampled by syringe extraction from the recirculating stream at different contact times, and injected into a gas chromatograph equipped with flame ionization and thermal conductivity detectors. An additional GC-MS was also employed to confirm the identity of reaction products.

The catalytic activity and product selectivities obtained on Cu/ZnO (30/70 at.%) during methanol and ethanol coupling reactions are shown in Fig. 4, 5. The results are summarized as follow:

a) The ethanol conversion reached an asymptotic value of about 60%. A methanol conversion level of about 13% was much lower than that of ethanol. The methanol and ethanol turnovers, calculated based on the total number of copper atoms, as a function of time are shown in Fig. 4.

b) Acetaldehyde, produced by ethanol dehydrogenation, was the primary product (Fig. 5). Only trace amounts of acetone (by acetaldehyde self-condensation), methyl formate, n-butyraldehyde (by acetaldehyde self-condensation), methyl acetate, and ethyl acetate (by acetaldehyde-ethanol condensation) were observed (Fig. 5). CO and H_2 were also formed from the decomposition of methanol. The detailed mechanism for these products formation will be discussed in the *Identification of Reaction Intermediate Section.*

The dehydrogenation and condensation reactions of ethanol were investigated on Cu/ZnO (30/70 at.%), Mg_5CeO_x, $Cu_{0.5}Mg_5CeO_s$ and $Cu_{0.5}Mg_5CeO_x$. The catalytic activity and product distribution obtained on Cu/ZnO at 250 °C are shown in Fig. 6 and 7 and summarized as follow:

a) The ethanol conversion reached an asymptotic value ~ 80%, indicating the reaction also approaches chemical equilibrium on this catalyst. Ethanol turnovers as a function of time is depicted in Fig. 6.

b) The main product was acetaldehyde, formed by dehydrogenation of ethanol (Figure 7).

c) The condensation products, present in small quantities, were acetone, n-butyraldehyde and ethyl acetate

Acetaldehyde, the most abundant product, appears to be a reactive intermediate and undergoes significant secondary reactions. The selective production of aldehyde from alcohol on copper-based catalysts has been reported since early 1970 (12,13). These authors found that on Cu metal catalysts saturated aliphatic alcohol yields considerable amounts of aldehyde and ester. The ester was believed to be formed by the reaction between an aldehyde and an alcohol. In our case, the formation of ethyl acetate is a result of ethanol-acetaldehyde condensation via a hemiacetal mechanism. Recently, several authors (14-16) have reported that alcohol adsorbs dissociatively on copper to form ethoxy species, which then decompose to form aldehyde. On the other hand, several studies on ZnO (16-19) have showed that ethanol decomposed to form ethylene, acetaldehyde and/or ethylene oxide. The formation of ethylene is due to the presence of anionic vacancies on low-coordinated Zn^{2+} sites. These sites are produced during catalyst pretreatment under reducing conditions. In our reaction conditions, no ethylene was observed, perhaps because of the low reaction temperature employed in this study. Ethylene was reported to appear in large quantities at temperatures greater than 300°C (16).

Mg_5CeO_x was inactive in ethanol dehydrogenation. The ethanol conversion reached a low value of about 7% as shown in Fig. 8, even though the reaction was carried out at a temperature 50 °C higher than that Cu/ZnO. It is surprising that the conversion leveled off at high contact time since the reaction was still far from equilibrium limitation. This might be due to CO_2 poisoning of basic sites or coordinately unsaturated sites. For a Cu-free Mg_5CeO_x sample, the basic sites of MgO are responsible for ethanol dehydrogenation. During the reaction, ethanol and its derivatives could react with the lattice oxygen from CeO_2 to form carbon oxides. The build-up of CO_2 during the reaction gradually decreased the number of basic sites available for dehydrogenation reaction. Thus, the activity decreased to zero. As shown in Fig. 9, the product distribution was similar to that obtained on Cu/ZnO.

Copper containing $CuMg_5CeO_x$ and K-$CuMg_5CeO_x$ (1 wt %) catalysts showed much higher activity than Mg_5CeO_x. The catalytic activities and product selectivities are illustrated in Fig. 10-13. The ethanol conversion reached an asymptotic value ~ 90% on both catalysts. Fig. 10 and 11 give ethanol turnovers as a function of contact time. This

result indicates the importance of Cu in ethanol dehydrogenation. Moreover, CO_2 has a weaker effect on copper activity than on MgO activity. Again, the main product was acetaldehyde, with small amounts of acetone, ethyl acetate, n-butyraldehyde, and β-keto-butanal.

No difference in the rate of acetaldehyde production was observed between the unpromoted and K-promoted catalyst. On the K-promoted catalysts the acetone production was higher than that of the unpromoted catalyst (Fig. 14 and Fig. 15, respectively).

3.2 Isobutanol Synthesis at High Pressure in CMRU

Unpromoted $Cu_{0.5}MgCe_2O_x$ and K-promoted $Cu_{0.5}MgCe_2O_x$ (Mg/Ce=0.5) were studied in CMRU-5, -6, -7; unpromoted $Cu_{0.5}Mg_5CeO_x$ and M-promoted $Cu_{0.5}Mg_5CeO_x$ (Mg/Ce=5, M=K,Cs) were studied in CMRU-8, -9, -10, -12, -13, -14, -15,-16. Catalysts with Mg/Ce=0.5 showed high selectivities to methanol (77.5-77.7%) and hydrocarbons (6.0-18.7%), and low selectivities to higher alcohols (2.8-3.0%). Low CO conversions (3.2-7.5%), which are less than those attainable at methanol synthesis equilibrium (18-25%), were attributed to the large amount of residual potassium in the unpromoted oxide (MG3-1 O). Apesteguia et al. [1] reported that the *total* alkali-content of $Cu/MgO/CeO_2$ should not exceed 1 wt.%. K-loading amounted to (*Table* 1) 4.1 wt.% in CMRU-5 (MG3-1 O) and 6.5 wt.% in CMRU-6 and -7 (MG3-1 O/K).

High selectivities to hydrocarbons on $Cu_{0.5}MgCe_2O_x$ with low selectivities to higher alcohols were attributed to the large amount of CeO_2 in these catalysts. $Cu_{0.5}MgCe_2O_x$ contains 64 wt.% Ce whereas the patented catalyst ($Cu_{0.5}Mg_5CeO_x$) [1] contains 34 wt.% Ce. Xu et al. [20] have reported an optimum Ce loading of 3-18 wt.% for Cu/ZnO-based catalysts. Low selectivities to higher alcohols in CMRU-5, -6, and -7 (Mg/Ce=0.5) suggest MgO, a stronger base than CeO_2, is responsible for the base-catalyzed condensation reactions leading to higher alcohols. Future synthesis of $Cu/MgO/CeO_2$ materials will address compositional optimization with respect to Cu/Mg and Cu/Ce ratios.

CMRU-8 and -9 used $Cu_{0.5}Mg_5CeO_x$ (MG3-1b O) and K-promoted $Cu_{0.5}Mg_5CeO_x$ (MG3-1b O/K), respectively, which match the literature catalysts [1] compositionally. The unpromoted catalyst was studied (CMRU-8) at 325 °C and 745 psi with GHSV = 1832 cm^3 (STP)/g.cat·h. The CO conversion was low (5.4%), and selectivities to methanol (87.8%) and hydrocarbons (11.2%) were high (*Table 2*). These results were similar to those obtained in CMRU-5, -6, and -7, but for reasons other than high K and Ce content. The catalyst bed was centered at the *bottom* zone of the furnace (half of the catalyst was *outside* of the furnace where the temperature was 200 °C). The top zone of the furnace was at 380 °C to achieve an average temperature of 320 °C in the reactor. The large temperature differential along the length of the reactor existed because the bottom zone of the reactor was heat-traced and well-insulated resulting in lower

temperatures at the bottom zone whereas the top zone of the reactor was not insulated. The high temperature in the top zone of the reactor caused the high selectivities to hydrocarbons in CMRU-8, whereas the low temperature in the bottom zone (where the catalyst was centered) caused the high selectivity to methanol with no higher alcohol formation. CMRU-9 and CMRU-10 were also unwittingly tainted with the large temperature differential problem.

CMRU-9 ($K\text{-}Cu_{0.5}Mg_5CeO_x$) resulted in the same conversion achieved by Apesteguia et al. (19.2%) [1], however, the methanol selectivity was very high at ~96.9% (*Table 2*). Increasing the reactor temperature by 20 °C and decreasing the space velocity from 1800 to 450 cm^3(STP)/g.cat·h decreased the methanol selectivity from 96.9% to 93.6% and increased the isobutanol selectivity from 0.2% to 0.6%. The low higher alcohols selectivities measured in CMRU-9 were erroneously attributed to a low potassium loading on the catalyst instead of to the low temperature (~250 °C) in the catalyst bed; therefore, CMRU-10 used a charge of 3 wt.% $K\text{-}Cu_{0.5}Mg_5CeO_x$, a three-fold increase in K-loading. The additional potassium on the catalyst resulted in a decreased conversion of 3.3% in CMRU-10 compared with CMRU-9 (19.2%). Decreasing the space velocity by a factor of two increased the conversion to 6.5%. Not surprisingly, catalyst performance did not reproduce that of the patent [1] in runs CMRU-8, -9, -10 (*Tables 2 and 3)*, seen in the high methanol and low higher alcohols selectivities. The large amount of insulation at the reactor effluent was removed in order to attain a uniform temperature along the length of the reactor. Subsequent reactor charging was performed with much greater care to ensure that the catalyst was confined to the center of the reactor and central furnace zones. These issues, therefore, do not taint subsequent CMRU data.

CMRU-12 and CMRU-13 used MG3-10b O/K and MG3-10 O/K, respectively. The difference between these catalysts is that MG3-10 b O/K ($K\text{-}Cu_{0.5}Mg_5CeO_x$) was impregnated with potassium *before* calcination to form the K-promoted mixed metal oxide while MG3-10 O/K ($K\text{-}Cu_{0.5}Mg_5CeO_x$) was impregnated with potassium *after* calcination of $Cu_{0.5}Mg_5CeO_x$. CMRU-12 gave a CO conversion comparable to that achieved in the patent [1] results (*Table* 4), however, alcohol selectivities show that methanol was formed to a greater extent and higher alcohols were formed to a lesser extent compared with patent [1] data (*Table* 4). The methanol/isobutanol ratio was 9.4 in CMRU-12 whereas the patented catalyst gave methanol/isobutanol=5.5. The high selectivity to methanol and low selectivities to ethanol, 1-propanol, and isobutanol in CMRU-12 compared with the patent data suggests that K-addition *before* calcination hindered the turnover of basic sites while Cu sites were unaffected (methanol formation rate in CMRU-12 is higher than that of the patent results). K-addition before calcination probably resulted in a higher potassium dispersion on this catalyst, which blocked basic sites to a greater extent than Cu sites because of the low Cu surface area (16.7 m^2/g) compared with the total surface area (162 m^2/g). The amount of total surface area associated with MgO is at least a factor of five higher than Cu based on a Cu/MgO sample (MG3-5 O) prepared in our laboratory, which had a surface area of 118 m^2/g.

CMRU-13 resulted (*Table* 4) in a higher CO conversion (20.8%), and hence, a slightly lower methanol/isobutanol ratio (5.0) compared to the patent data. The lower methanol formation rate in the patent data (*Table 4*) compared with CMRU-12 and CMRU-13 derives from much higher CO_2 and hydrocarbon formation rates, evidenced by the fact that while conversions are similar in the patent and CMRU-12 data, CO_2 and hydrocarbons selectivities are higher in the former. Interestingly, selectivities to hydrocarbons were very low in CMRU-13 compared to patent data, resulting in a much higher alcohol/hydrocarbon ratio in the CMRU data.

Apesteguia et al. [1] reported data at 290 °C, 320 °C, and 360 °C. The highest temperatures studied in CMRU-12 and CMRU-13 were 360 °C and 331 °C, respectively. A direct comparison at higher temperatures is not possible because conversions are not comparable; the data (*Table 5*), however show expected selectivity shifts at the higher temperatures - lower methanol with higher isobutanol and hydrocarbon selectivities. The patent data [1] shows that conversion did not change appreciably with increasing temperature: conversions were 19.9%, 15.5%, and 19.0% at 290, 320, and 360 °C, respectively. We observed, however, large decreases in conversion with increasing temperature at the same space velocity. For CMRU-12, conversions were 14.4% (320 °C), 8.0% (341 °C) and 4.1% (362 °C) at 1790 cm^3(STP)/g.cat·h ; for CMRU-13, conversions were 20.8% (320 °C) and 6.8% (331 °C) at 1810 cm^3(STP)/g.cat·h. The conversion decrease with increasing temperature in the CMRU data (*Table 5*) was not the consequence of catalyst deactivation, but rather CO_2 inhibition of K^+ and basic sites (*discussed later*), which leads to both decreased methanol and branched alcohol formation rates. Low hydrocarbon formation in CMRU data compared with the patent data (*Table 5*) is even more pronounced at higher temperatures. Methanol and isobutanol formation rates in CMRU-12 at 362 °C were lower than those of the patent by a factor of two while the hydrocarbon formation rate was lower by a factor of ten.

CMRU-14 used Cs-$Cu_{0.5}Mg_5CeO_x$ (MG3-10 O/Cs) in order to learn if Cs was a more effective promoter than K in the formation of higher alcohols. This material was derived from the same mixed metal oxide (MG3-10 O) used in CMRU-13, but was impregnated with Cs instead of K. The low CO conversion (*Table 6*) of CMRU-14 (Cs-promotion) compared with CMRU-13 (K-promotion) might be caused by 1) too high a Cs-addition, or 2) the larger size of the Cs^+ cation, which covers a higher fraction of the surface than does K^+ at the same loading. Irreproducibility in alkali-loading has been shown a significant cause for CO conversion variability in the CMRU data, and therefore, highlights the former possibility as most likely.

CMRU-14 results (*Table 6*) show that CO conversion (9.0%) was a factor of two lower than that obtained in CMRU-13 (20.8%). The methanol formation rate was a factor of three lower while the ethanol formation rate was slightly higher in CMRU-14 compared with CMRU-13. Methanol and isobutanol formation proceed by the following parallel-series reactions [11, 21]:

$$CO + H_2 \rightleftharpoons C_1^* \rightleftharpoons CH_3OH \quad (1)$$

$$\downarrow \text{basic oxide}$$

$$CH_3CH_2OH + H_2O$$

$$C_1^* + CH_3CH_2OH \xrightarrow{\text{basic oxide}} CH_3CH_2CH_2OH + H_2O \quad (2)$$

$$C_1^* + CH_3CH_2CH_2OH \xrightarrow{\text{basic oxide}} (CH_3)_2CHCH_2OH + H_2O \quad (3)$$

$$CO + H_2O \rightleftharpoons CO_2 + H_2 \quad (4)$$

Ethanol forms from both 1) CO/CO_2 hydrogenation, coupling, and condensation and from 2) methanol dehydrogenation, coupling, and condensation. In either case, basic sites are needed to form ethanol because coupling and condensation reactions occur, producing one molecule of H_2O for each molecule of CH_3CH_2OH. Because basic sites promote ethanol formation as well as 1-propanol and isobutanol formation, one cannot conclude that basic sites were less effective on the Cs-promoted catalyst (CMRU-14) compared with the K-promoted catalyst (CMRU-13) because the ethanol formation rate was slightly higher in CMRU-14. Cs-$Cu_{0.5}Mg_5CeO_x$ was a more effective catalyst with respect to the rate-limiting step of ethanol formation [5] than K-$Cu_{0.5}Mg_5CeO_x$ because methanol was converted to ethanol three times faster in CMRU-14 compared with CMRU-13.

Slaa et al. [8] have reviewed product distributions obtained on modified methanol synthesis catalysts (M-Cu/ZnO/A_x, M=Cs, K, A_x=alkaline earth oxides). These authors concluded that the C_1 to C_2 step in methanol/higher alcohol synthesis is rate-limiting and that doping Cu/ZnO with alkali and alkaline-earth oxides capable of forming positive surface centers activates C_1 to C_2 formation. CMRU-14 results show that cesium was more effective in activating the C_1 to C_2 step than potassium (CMRU-13). The low 1-propanol and isobutanol formation rates in CMRU-14 suggest that 1) ethanol formation is not the only bottleneck in isobutanol synthesis, and 2) basic sites which promote C_2 formation (C_1·C_1 coupling) are different from those which promote C_{3+} alcohols (C_1·C_{2+} coupling).

CMRU-13 (320 °C), CMRU-13B (331 °C), and CMRU-14 (320 °C) included a study in the effect of space velocity on CO conversion and product distribution. CMRU-13 showed (*Figure 16a*) a two-fold increase in conversion over a four-fold decrease in space velocity while CMRU-13B and CMRU-14 showed (*Figure 16b,c*) that conversion was independent of space velocity over the entire range studied (GHSV=900-3600 cm^3(STP)/g.cat·h). Decreasing the space velocity from 1800 to 900 cm^3(STP)/g.cat·h resulted in a conversion increase from 21 to 24% in CMRU-13, however, the increased conversion did *not* result in increased higher alcohol selectivities (*Figure 17*): methanol was converted instead to DME. CMRU-13B (*Figure 18*) and CMRU-14 (*Figure* 19) showed this same behavior at the space velocity change from 1800 to 900

cm^3(STP)/g.cat·h: higher alcohol selectivities decreased while DME + hydrocarbon and CO_2 selectivities increased. The difference, however, between these runs (*Figures 18,19*) and CMRU-13 (*Figure 17*) is that the CO conversion was independent of space velocity. Patent results [1], however, show that selectivities to isobutanol and 2-methyl-1-butanol increased with decreasing space velocity (*Table 7*) while selectivities to linear alcohols did not change appreciably.

Table 7. Effect of Space Velocity on Alcohol Selectivities-Patent Results [1]

GHSV			Alcohol Selectivities[a] (%C)			
(cm^3(STP)/g.cat*h)	methanol	isobutanol	ethanol	1-propanol	1-butanol	2-me-1-butanol
1850	89.0	5.8	1.7	2.2	0.1	0.7
920	85.8	8.5	1.6	2.3	0.2	1.0
460	81.7	12.1	1.5	2.3	0.2	1.3

[a]0.9 wt.% K-$Cu_{0.5}Mg_5CeO_x$ at 290 °C, 50 atm, H_2:CO=1

These authors [1] did not report conversions for the above study (*Table 7*). The observation that conversion did not increase with decreasing space velocity suggests that methanol synthesis was at equilibrium in CMRU-13B and CMRU-14, however, comparison of equilibrium and CMRU conversions (*Table 8*) shows that CMRU-13B and CMRU-14 resulted in *lower* conversions than those predicted by methanol synthesis equilibrium.

Table 8. CO Equilibrium Conversions to Methanol for H_2:CO=1

Run	T	P	X (equilibrium)	X (actual)
	(°C)	(atm)	(%)	(%)
CMRU-13	320	50	15.1	24.8
CMRU-13B	331	50	12.6	7.5
CMRU-14	320	50	15.1	9.2

Figures 17, 18, and 19 show that decreasing space velocities promote higher DME and hydrocarbon selectivities while the isobutanol selectivity decreased (*Figure 17*), or remained constant (*Figures 18 and 19*). DME forms by methanol coupling with dehydration: one molecule of H_2O is produced for each molecule of DME formed. The produced water can react via WGS to give CO_2. Zhang et al. [22] showed that the pre-adsorption of CO_2 and H_2O on MgO resulted in decreased activities for butyraldehyde self-condensation. This result was attributed to the titration of basic sites on MgO, which are responsible for condensation reactions [22]. The increase in DME and CO_2 selectivities at low space velocities may be responsible for the inhibition of branched alcohol formation because 1) increases in H_2O and CO_2 disfavor further condensation reactions, and 2) increases in H_2O and CO_2 may inhibit basic sites.

CMRU-13 data (*Figure 17*) shows that the methanol formation rate (product of conversion and methanol selectivity) increased with decreasing space velocity while CMRU-13B (*Figure 18*) and CMRU-14 (*Figure 19*) data show constant rates of methanol formation at the lower space velocities. Methanol formation rates have been shown higher on alkali-promoted Cu/ZnO [23] compared to unpromoted Cu/ZnO. Vedage et al. [23]

proposed a Cs-formate precursor to explain the increased methanol synthesis rate on CsOH/Cu/ZnO. CMRU-13B and CMRU-14 results suggest that the sites where methanol formed, either Cu-formate or alkali-formate, as well as basic sites were inhibited at low space velocities because the product distributions in these runs did not change with decreasing space velocity. These results might be caused by H_2O and CO_2 reversible titration of K^+ (CMRU-13B) and Cs^+ (CMRU-14), which would inhibit methanol formation, and H_2O and CO_2 reversible titration of basic sites on MgO, which would inhibit condensation reactions leading to higher alcohols. In order to learn more about the effect of CO_2 on these catalysts, we considered the CO_2 partial pressure and its effect on reaction rate (*Figure 20*) in CMRU-13, -13B, and 14.

In CMRU-13, activity increased by a factor of two for a P_{CO2} decrease from 10.5 to 6.0 psi (*Figure 20a).* CMRU-13B showed (*Figure 20b)* an activity which was only one-fifth of that measured in CMRU-13 at P_{CO2}=6.0 psi , and further, the activity sharply decreased with increasing P_{CO2}. CMRU-14 resulted in (*Figure 20c*) P_{CO2}=8.0 psi at the start of the run, but activity decreased throughout the remainder of the run, independent of P_{CO2}. The effect of CO_2 on reaction rate is ambiguous in CMRU-14 while increased CO_2 partial pressures resulted in decreased activities in CMRU-13 and -13B. This effect was more pronounced in the higher temperature run, CMRU-13B, even though the CO_2 pressure was lower in CMRU-13B. Future experiments will involve a close examination of the threshold CO_2 pressure for these catalysts.

A new batch of K-$Cu_{0.5}Mg_5CeO_x$ (MG3-11 O/K) was used in CMRU-15. This catalyst resulted in a very low conversion (2.3%) at T=320 °C, P=44 atm, H_2/CO=1, and GHSV=6100 cm^3(STP)/g.cat·h while the methanol and isobutanol selectivities were comparable to those of CMRU-12 and CMRU-13 (*Table 9*). The low conversion was attributed to the three-fold decrease in surface area for MG3-11 O/K compared with MG3-10 O/K. The low surface area was probably due to an incomplete washing step in which MgO did not convert to $Mg(OH)_2$ [24] and to the K-addition step, which would result in too high a K-loading after incomplete washing.

CMRU-16 (*Table 9*) was run with unpromoted $Cu_{0.5}Mg_5CeO_x$ (MG3-11 O) in order to determine if the K-addition step to this material was responsible for the low conversion in CMRU-15. The conversion in CMRU-16 was also low at 3.2%. Apesteguia et al. [1] show that their unpromoted $Cu_{0.5}Mg_5CeO_x$ resulted in X_{CO}=21% at T=320 °C and P=50 atm. It is known that the surface area of MgO increases by a factor of 10 upon heating in water (MgO converted to $Mg(OH)_2$) [24]. The precursor solids used in CMRU-15 and -16 were re-washed in hot de-ionized water. Calcination of this material resulted in S.A.=167 m^2/g, a value comparable to those obtained for the MG3-10 catalysts. Future synthesis of these catalysts will use a thorough washing step to remove the residual potassium left during co-precipitation and to promote the increased MgO surface area.

CMRU-18 will use a charge of the re-washed MG3-11 O. Before conducting this experiment, however, we will re-charge the BASF Cs-$Cu/ZnO/Al_2O_3$ catalyst (CMRU-

17) in order to determine the effect of CO_2 partial pressure on activity. CO_2 will be added to the H_2/CO/Ar feed in a range of concentrations ($2 \cdot P_{CO2}$-$5 \cdot P_{CO2}$, where P_{CO2} is the steady-state synthesis value at 300 °C, 45 atm, GHSV=1250 cm^3(STP)/g.cat.h). Since MgO is a stronger base than ZnO, we expect that Cs-Cu/ZnO/Al_2O_3 will show a greater tolerance for CO_2 than do the Cu/MgO/CeO_2 materials. This run will be useful, however, in determining the protocol for CO_2 addition.

Future runs will use catalysts containing higher Cu and lower Ce. Higher Cu content is expected to give larger Cu particles, enhanced methanol formation rates, and hence, enhanced $C_1 \cdot C_{2+}$ condensation reaction rates. Lower Ce is expected to result in larger Cu particles (lower Cu dispersions) and lower DME and hydrocarbon formation rates.

Task 4: Identification of Reaction Intermediates

During this reporting period, a LV10K fine control leak valve was installed in front of the mechanical pump in order to reduce the amount of samples extracted by the pump. The lower pumping rate results in 1) an increase in the inlet pressure of the mass spectrometer, and consequently an enhanced sensitivity of mass spectrometer, and 2) slightly broadened peaks during pulse injection. Therefore, more data points can be taken for each peak, yielding reproducible peak intensity.

4.1. Determination of Copper Surface Area

Copper surface area was determined by Cu surface atom titration at 90 °C using N_2O introduced by pulse injection. The amount of N_2O injected through a sample loop was consistent with that determined based on peak area.

In a typical experiment, a 80-140 mesh sample (~33.0 mg) was loaded into a 6 mm-i.d. U-shape quartz reactor and pretreated in flowing helium at 450 °C for 20 min to remove carbonates and water prior to reduction in hydrogen stream (5 % H_2 in He) at 350 °C for 30 min. The temperature programmed reduction (TPR) of a Cu/MgO/CeO_2 catalyst indicated that copper reduction took place in the temperature range of 220-280 °C. After H_2 reduction, reaction temperature was lowered to 90 °C in a helium flow and nitrous oxide was then introduced by pulse injection through the sample loop. As reported in the literature [25,26], the optimum titration temperature was 85 °C - 95 °C, at which the oxidation of copper by N_2O is sufficiently mild that only the surface copper is oxidized and only to the Cu(I) oxidation state. At temperatures > 120 °C, bulk oxidation of copper will occur. Low temperature may cause the incompleteness of surface reaction since this is an activated process with an apparent activation energy of 0-2 kcal/mol [27].

For a freshly reduced Cu/MgO/CeO_2 sample, the first few pulses of nitrous oxide titration (5 % N_2O balanced in helium) led to the evolution of gas-phase N_2; the oxygen

atoms remained chemisorbed on the surface. Upon further addition of nitrous oxide, a m/e 44 peak of unreacted N_2O was evolved. Once the mass 44 peak intensity remained constant for subsequent pulses, the reaction was completed. Based on the amount of N_2O consumed or the amount of N_2 formed, the total number of oxygen atoms chemisorbed on the surface can be determined. It should be pointed out that no gas-phase oxygen was observed during pulse injection, indicating all the oxygen atoms from N_2O remained on the surface. As one oxygen atom corresponds to a copper area of 2 X 10^{-19} m^2 [27], the copper surface area of a $Cu/MgO/CeO_2$ (MG3-1bO) catalyst was found to be *ca.* 34.6 m^2/g-cat. The copper surface areas of potassium modified $Cu/MgO/CeO_2$ samples were 13.9 m^2/g-cat for MG3-1bO/K, and 16.6 m^2/g-cat for MG3-10bO/K. These two catalysts have the same potassium loadings but were prepared by incipient wetness via different precursors. Copper dispersions, defined as the ratio of the number of surface copper atoms to the total number of copper atoms in the catalyst, were 48% and 19% for MG3-1bO and MG3-1bO/K, respectively. The dramatic decrease in copper surface area cannot be explained by the change in total surface area because the addition of potassium caused only a slight change in total surface area. For example, the total surface area determined by N_2 at -196 °C decreased from 108 m^2/g for MG3-1bO to 88 m^2/g for MG3-1bO/K. Interestingly, the total surface area of MG3-10bO/K, which is 162 m^2/g, is even higher than that of MG3-1bO. The lower copper surface areas at higher potassium loadings might be due to the inability to reduce Cu^{2+} to Cu^0 completely. In a series studies on unsupported alkali-promoted copper catalyst, King and co-workers [28-30] have found that upon H_2 reduction at 275 °C, only part of the Cu^{2+} species in the calcined catalyst was reduced to copper metal, with the remaining being in the Cu^+ state. The alkali-free copper samples, however, were completely reduced to copper metal. The stabilization of Cu^+ during Cu^{2+} reduction was believed to be due to the formation of $K^+Cu^+CO_3$ species.

MgO/CeO_2, subject to H_2 reduction at conditions similar to that of $Cu/MgO/CeO_2$, did not decompose nitrous oxide at 90 °C. Thus, only copper was responsible for N_2O consumption. The addition of potassium significantly reduced copper exposure perhaps because of the deposition of potassium compounds on the surface which block the copper sites or promote alkali-induced sintering.

Reduction temperature also has an effect on copper surface area. For example, a $Cu/MgO/CeO_2$ sample, prereduced at 260 °C for 30 min yielded a copper surface area of about 24.8 m^2/g-cat, which is lower than 34.6 m^2/g-cat obtained on the sample prereduced at 350 °C. This indicates that copper reduction is not complete at 260 °C after 0.5 h. The Cu dispersions in these samples (19-48 %) are among the highest reported in the literature for Cu-based methanol and higher alcohol synthesis catalysts.

Cu/MgO, with the same amount of Cu as in $Cu/MgO/CeO_2$, has a copper surface area of about 12.3 m^2/g-cat and a copper dispersion of about 16 %, in contrast to the respective value of 34.6 m^2/g and 48 % for copper surface area and dispersion on $Cu/MgO/CeO_2$. The total surface area of these two samples are comparable, with 108 m^2/g-cat for $Cu/MgO/CeO_2$ and 118 m^2/g-cat for Cu/MgO. The onset of Cu/MgO reduction by H_2 was 185 °C, which is lower than the value of 220 °C observed on

$Cu/MgO/CeO_2$. Similarly, the peak maxima are 220 °C and 255 °C for Cu/MgO and $Cu/MgO/CeO_2$, respectively. This suggests that Cu^{2+} ions on $Cu/MgO/CeO_2$ are more difficult to reduce than those on Cu/MgO. The increase in Cu^{2+} reduction temperature and copper dispersion may reflect a strong metal-support interaction between copper and cerium oxide. In the case of Rh^{2+}, Anderson and co-workers [31] have reported that rhodium ions on ceria surface were stabilized against reduction and aggregation by incorporation of the Rh cations to cerium oxide surface layers, resulting in a high metal dispersion. The same phenomenon has been observed with Cu^{2+} ions on ceria surface [2,32]. Lamonier et al. [2] have demonstrated that the insertion of Cu^{2+} into the ceria lattice occurred during the coprecipitation step of catalyst preparation, resulting the creation of anionic vacancies upon calcination. Four different copper species attributed to monomers, dimers, clusters and small particles of CuO have been found. The metal-support interaction, however, is believed to be stronger between Rh^{2+} species and ceria than that between Cu^{2+} and ceria. It was found that Rh^{2+} species were stable, whereas Cu^{2+} ions on cerium oxide were reduced after H_2 treatment at 500 °C.

4.2. TPSR of Acetaldehyde and Ethanol over $Cu/MgO/CeO_2$ Catalysts

The temperature programmed surface reactions of ethanol and acetaldehyde have been studied in detail using a combination of gas chromatograph and mass spectrometer for the analysis of the evolved products. The desorption products were monitored continuously using a mass spectrometer. At the same time, the products at different temperatures were analyzed by GC-MS through syringe sampling. During a typical TPSR experiment, a prereduced fresh sample was saturated with the oxygenate of interest at room temperature for 10 min. It was then purged with helium to remove gas-phase and weakly adsorbed species, and the run was started by letting the reactor temperature increase at 30 °C/min to 450 °C.

4.2.1. Acetaldehyde TPSR

The desorption products observed on MgO/CeO_2, $Cu/MgO/CeO_2$ and K-$Cu/MgO/CeO_2$ are shown in Fig. 21, the major desorption features are the evolution of acetaldehyde, crotonaldehyde (m/e 70) and water with peak maxima at about 90 °C. Self-condensation of acetaldehyde on basic sites results in the formation of 3-hydroxybutanal, which undergoes subsequent dehydration reaction leading to a crotonaldehyde-to-water ratio of 1.

$$2\,CH_3\text{-}CHO \rightarrow CH_3\text{-}\underset{\displaystyle OH}{\underset{|}{C}}H\text{-}CH_2CHO \longrightarrow CH_3\text{-}CH{=}CH\text{-}CHO + H_2O \qquad (1)$$

Water resulting from surface hydroxyl species is responsible for the tailing water peak at high temperatures. MgO, a strong basic oxide, is inactive in dehydration reaction because of its lack of acid sites. Kita and co-workers [33] have reported in the self-condensation

of n-butyraldehyde on MgO, that the main product was 2-ethyl-3-hydroxyhexanal, and the selectivity to 2-ethyl-2-hexanal, the dehydration product, was less than 2 %. Addition of γ-Al_2O_3, an acidic oxide, increased 2-ethyl-2-hexenal yield at the expense of 2-ethyl-3-hydroxyhexanal. Since crotonaldehyde was formed on both MgO/CeO_2 and $(K)Cu/MgO/CeO_2$, sites associated with CeO_2 might be responsible for its formation. The highly dehydroxylated cerium oxide pretreated under reducing atmosphere may contain oxygen vacancies and coordinately unsaturated cerium ions exhibiting Lewis acidity [34]. The insertion of lower-valance cations such as Cu^{2+} and Mg^{2+} into ceria lattice also leads to the creation of anionic vacancies. These anionic vacancies can be titrated by surface hydroxyl species formed in dehydration reactions.

A major difference between MgO/CeO_2 and $(K)Cu/MgO/CeO_2$ is that the latter desorbs of methyl ethyl ketone (MEK) at ~ 170 °C, as shown by the evolution of species with m/e 72, 43 and 29 in this temperature range. MEK was not observed on MgO/CeO_2. Its formation has been further confirmed by GC-MS analysis of the desorption products. Another significant feature of $(K)Cu/MgO/CeO_2$ is the formation of acetone at both 180 °C and 360 °C. The amount of acetone produced on MgO/CeO_2 is an order of magnitude less than that on $(K)Cu/MgO/CeO_2$, indicating a critical role of copper in MEK and acetone formation. The precursor of methyl ethyl ketone and low-temperature acetone might be 3-hydroxybutanal formed via self-condensation of surface acetaldehyde species. As will be discussed in the case of ethanol, alcohol dehydrogenation takes place readily at 170 - 180 °C over copper metal. Thus, at these temperatures 3-hydroxybutanal could undergo either dehydration, as evidenced by the continuous production of crotonaldehyde up to 200 °C (Fig. 21), or dehydrogenation on copper metal to form 3-oxobutyraldehyde as shown by reaction 2:

$$CH_3\text{-}\underset{\displaystyle OH}{\underset{|}{CH}}\text{-}CH_2CHO_{(a)} \xrightarrow{Cu} CH_3\text{-}CO\text{-}CH_2\text{-}CHO + 1/2H_2 \qquad (2)$$

The formation of 3-oxobutyraldehyde on $Cu/MgO/CeO_2$ catalysts, though in small quantity, has been confirmed by GC-MS. 3-oxobutyraldehyde could either react with lattice oxygen from the reducible metal to form acetoacetate, or produce methyl ethyl ketone and an oxygen atom. The oxygen species could migrate and heal a surface anionic vacancy. Since acetoacetic acid is not stable and undergoes decarboxylation readily at temperatures of 100 - 150 °C [35], it is expected that acetoacetate, once formed, will decompose to acetone. The reaction pathways of 3-oxobutyraldehyde are illustrated as follow:

$$CH_3\text{-}CO\text{-}CH_2\text{-}CHO_{(a)} + O_s \rightarrow CH_3\text{-}CO\text{-}CH_2\text{-}COO_{(a)} + H_{(a)} \rightarrow CH_3COCH_3 + CO_2 \qquad (3)$$

$$CH_3\text{-}CO\text{-}CH_2\text{-}CHO_{(a)} + 2\,H_{(a)} \rightarrow CH_3\text{-}CO\text{-}CH_2\text{-}CH_3O_s \qquad (4)$$

A similar mechanism for MEK formation on $Cu/ZnO/Al_2O_3$ has been proposed by Pennella et al. [11].

The acetone formed at 380 °C, however requires a different pathway because none of the intermediates in the above mechanism are likely to survive at these high temperatures. Surface acetate species, formed by the nucleophilic attack of the carbonyl group of acetaldehyde by electronegative O^{2-} from reducible metal oxides, is likely to be responsible for the formation of these high-temperature species. The formation of acetone at T > 300 °C has also been reported by Prieto and co-workers in TPSR studies of acetic acid on TiO_2 [36]. They proposed that a bimolecular reaction involving ketene and molecularly adsorbed acetic acid in equilibrium with the gas phase leads to the formation of acetone:

$$CH_2=C=O + CH_3COOH_{(a)} \longrightarrow CH_3COCH_3 + CO_2 \qquad (5)$$

No gas-phase ketene was observed on this catalyst. They believed that ketene, once formed, remains strongly adsorbed on coordinately unsaturated Ti^{4+} sites. It should be pointed out that the presence of gas-phase ketene has been observed during the temperature-programmed surface reactions of acetic acid and acetaldehyde on Cu (37) and ZnO (38).

In the TPSR of acetaldehyde on (K)Cu/MgO/CeO_2 and MgO/CeO_2, however, no gas-phase ketene was observed. In analogy with Ti^{4+}, the ketene formed could be strongly adsorbed on the coordinately unsaturated Ce^{4+} sites. A mechanism similar to that proposed by Prieto et al. [36] may account for the formation of high-temperature acetone on (K)Cu/MgO/CeO_2. Yet, molecularly adsorbed acetic acid is less likely to exist in our study due to the basic properties of our catalyst and to the absence of gas-phase acetic acid. Therefore, ketene and surface acetate species instead of acetic acid might be the precursors of the high-temperature acetone. The presence of basic site enhanced acetone production; therefore, it is possible that $^-CH_2COO_{(a)}$ species, formed via α-H abstraction of acetate by a strong basic site, attacks the carbonyl group of ketene, leading to the formation of acetone:

$$CH_2=C=O + {}^-CH_2COO_{(a)} + 2H_{(a)} \longrightarrow CH_3COCH_3 + CO_2 \qquad (6)$$

Since the acidity of the α-hydrogen in acetate ions is weaker than that of α-hydrogen in acetaldehyde, only strong basic sites such as alkali metal oxide are able to break the C-H bond of acetate. The formation of very small amounts of acetone over Cu, ZnO and MgO/CeO_2 is not surprising because they lack strong basic sites. Cu promotes ketene production, whereas alkali metal oxides favor $^-CH_2COO_{ad}$ formation. The co-existence of Cu and strong basic sites greatly enhances the rate of acetone production. The hydrogenation of acetone leads to the formation of isobutanol observed in the high-pressure syngas-to-isobutanol reactions. As shown in Fig. 21, the amount of high-temperature acetone produced on K-promoted Cu/MgO/CeO_2 is twice as much as that on Cu/MgO/CeO_2; whereas, the low-temperature acetone, whose formation did not require

the strong basic sites, was comparable on these two catalysts. The potassium content in K-Cu/MgO/CeO_2, determined by atomic absorption, is 1.5 wt % in comparison to 0.4 wt % in Cu/MgO/CeO_2. Although its presence is necessary for acetone formation, excess potassium could block ceria, and therefore decrease the concentration of surface $CH_3COO_{(ad)}$ species, whose formation requires the presence of lattice oxygen from the reducible metal oxide. Moreover, the presence of potassium appears to reduce the dispersion of copper and thus decrease the rate of ketene formation. Thus, it is necessary to optimize potassium loading in order to achieve a high yield of higher oxygenates.

The high-temperature evolution of H_2, H_2O and CO_x may arise from decarboxylation of residual acetate:

$$CH_3COO_{(a)} \longrightarrow CH_{3(a)} + CO_2 \qquad (7)$$

This reaction has been reported to take place to a considerable extent on Cu (37) and ZnO (38). Reactions of ketene with surface oxygen species could also lead to the formation of surface hydrocarbon species (37).

$$CH_2{=}C{=}O_{(a)} + O_s \longrightarrow CH_{2(a)} + CO_2 \qquad (8)$$

Further reactions of these surface hydrocarbon residues at high temperatures can generate H_2, H_2O and CO_x.

Since both H_2 and CO are the reactants in the catalytic conversion of syngas to isobutanol, it is of interest to study their effects on aldol-condensation reactions. TPSR studies with H_2 or CO in the He carrier gas were carried out on (K)Cu/MgO/CeO_2 catalysts. As shown in Fig. 22, the addition of H_2 during acetaldehyde TPSR produced an acetaldehyde peak at about 390 °C in addition to the one previously observed at 90 °C in He carrier gas to form acetaldehyde in a reactive desorption step. This might be attributed to the reduction of surface ketene species by H_2:

$$CH_2{=}C{=}O_{(a)} + H_2 \longrightarrow CH_3CHO \qquad (9)$$

The formation of CO is a result of water-gas shift reaction:

$$CO + H_2O \rightleftharpoons CO_2 + H_2 \qquad (10)$$

This accounts for the observed decrease in CO_2 production when CO was added to the carrier gas (Fig. 22). Water was formed via dehydroxylation of surface hydroxyl species. Another interesting feature is the appearance of ethanol at 100-200 °C when H_2 is added; this ethanol evolution arises from the hydrogenation of acetaldehyde.

The presence of CO during acetaldehyde TPSR inhibits acetone formation because of the formation of CO_2 via water-gas shift reaction. CO_2 is likely to block the strong basic sites necessary for aldol condensation reactions.

4.2.2. Ethanol TPSR

Ethanol adsorbs dissociatively on the surface to form surface ethoxide species over Cu (15) and metal oxides (17, 18, 39). Based on literature results and our current observation, the schematic diagram of ethanol adsorption and reactions on metal-oxide and copper-containing catalyst surfaces is illustrated below:

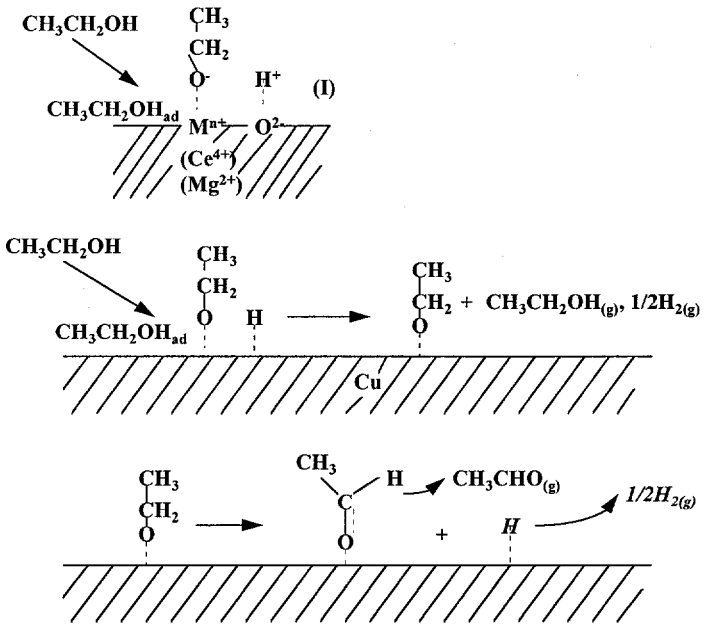

Fig. 23. Schematic Diagram of Ethanol adsorption and Reactions on Catalyst Surface

On metal oxides such as CeO_2 and MgO, the abstracted protons react with lattice oxygen to form water. Hydrogen atoms formed during dissociative adsorption of ethanol on copper can either recombine with ethoxide to form ethanol, or react with another H atom to produce H_2. Upon heating, most of the ethoxide species desorb as ethanol via recombination with surface hydrogen. The remaining ethoxide may either react with lattice oxygen on metal oxides to form surface carboxylic species or undergo α-H scission with the help of Cu to form acetaldehyde. The resulting surface hydrogen recombines to produce more H_2. As shown in Fig. 24, acetaldehyde and H_2 were produced in large quantities on Cu-containing catalysts, and acetaldehyde production reached a maximum at 180 °C. However, at T < 180 °C the rate of H_2 production is higher than that of acetaldehyde. As illustrated in the above schematic diagram, there are two hydrogen sources with one from O-H bond breaking and the other from C-H bond cleavage. This may explain the appearance of two hydrogen peaks in the temperature

range of 100-200 °C. The first H_2 peak, which appeared at a temperature similar to that of ethanol, resulted from surface H atoms produced via O-H rupture. The second H_2 peak, evolved at approximately the same temperature range as acetaldehyde, is attributed to C-H bond cleavage. These results suggest that the formation of H_2 and acetaldehyde from surface ethoxide species is reaction-limited. It is noteworthy that in the TPSR of ethanol over Cu(110) single crystal carried out by Madix et al. [15], the desorption temperature of H_2 was about 25 °C higher than that of acetaldehyde. Thus, they concluded that the formation of H_2 is desorption-limited.

The TPSR of ethanol over MgO/CeO_2 yielded small amounts of H_2, indicating the importance of Cu in ethanol dehydrogenation. The amount of H_2 produced on K-promoted $Cu/MgO/CeO_2$ is lower than that on unpromoted $Cu/MgO/CeO_2$. This is in agreement with the lower copper surface area observed on $K\text{-}Cu/MgO/CeO_2$. Potassium compounds could cover Cu surface, resulting in fewer copper surface atoms available for dehydrogenation reactions. Once acetaldehyde is formed, it will react with lattice oxygen from reducible metal oxides to form surface acetate species, which undergoes subsequent reactions leading to the formation of acetone as discussed in the case of acetaldehyde. It is noteworthy that the amount of acetone produced, however, is less than that in acetaldehyde TPSR. The peak temperature shifted to 380 °C and 400 °C over $Cu\text{-}MgO/CeO_2$ and $K\text{-}Cu/MgO/CeO_2$, respectively. Moreover, acetone formed on $K\text{-}Cu/MgO/CeO_2$ is less than that on $Cu/MgO/CeO_2$. These effects are attributed to the lower acetaldehyde production on lower copper surface area catalyst, which results in a decrease in the concentration of adsorbed acetone precursors. In contrast to acetaldehyde TPSR, only tiny amounts of crotonaldehyde and acetoacetaldehyde were produced (Fig. 24).

On Cu/MgO, the amount of ethanol desorbed is less than that on $Cu/MgO/CeO_2$ (Fig. 25), even though the surface areas of these two samples are comparable. On Cu/MgO, only small amounts of acetone are formed (20 % as much as that on $Cu/MgO/CeO_2$). It is even smaller compared to that produced on $K\text{-}Cu/MgO/CeO_2$. This is not surprising because of the lack of reducible metal oxide on Cu/MgO. As discussed above, surface acetate species, formed by reaction between acetaldehyde and lattice oxygen from reducible metal oxide, is a precursor for acetone production.

The effects of H_2 and CO on acetone production have also been studied during ethanol TPSR and the results are shown in Fig. 26. The addition of H_2 to the carrier gas stream increased CO and H_2O production and decreased CO_2 formation because of water-gas shift reaction. The presence of H_2 shifted the equilibrium of reaction 10 to the left, thus favoring CO and H_2O formation. In addition to the peak at 100-200 °C, an acetaldehyde peak at 380 °C was also observed. Its formation was a result of ketene reduction by H_2. Interestingly, no crotonaldehyde or methyl ethyl ketone was formed in the temperature range of 150 °C-250 °C on $K\text{-}Cu/MgO/CeO_2$. Instead, they evolved at about 390 °C. Aldol condensation of acetaldehyde species formed at 380 °C are responsible for crotonaldehyde and MEK formation. The presence of H_2 also increased acetone production. This is a result of several factors. First, H_2 decreased CO_2

production via water-gas shift reaction, therefore more surface strong basic sites remain available for aldol condensation reaction leading to the formation of acetone. Apparently, CO_2 will block the strong basic sites due to its acidic character. In addition, hydrogenolysis of the acetone coupling products such as acetone dimers and trimers on the surface lead to the formation of additional acetone during TPSR.

The addition of CO to the carrier 1) increased H_2 and CO_2 at T > 200 °C because of water-gas shift reaction, 2) caused a dramatic decrease in acetone production and 3) decreased H_2 production at temperatures below 200 °C. As illustrated in ethanol adsorption diagram (Fig. 23), during the adsorption of ethanol at room temperature, some will be adsorbed on the surface intact, while the other may undergo dissociatively adsorption. Upon heating, some of the molecularly adsorbed ethanol may dissociate via O-H bond cleavage on the surface. The dissociation of ethanol and decomposition of surface ethoxide species require the presence of unoccupied surface sites to accommodate H species. During ethanol TPSR in the presence of CO, however, all the sites unoccupied by ethanol will be occupied by CO. The dissociation reactions leading to ethoxide, H and acetaldehyde are unfavorable because no sites are available to accommodate H atoms. This results in fewer available gas-phase H_2 and surface intermediate species for acetone formation. The amount of ethanol produced is slightly higher when CO is added than that in the presence of either H_2 or pure He. Since CO_2 was produced via water-gas shift reaction in the presence of CO, more strong basic sites were blocked. Thus, the rate of aldol condensation reactions leading to acetone was decreased. Because acetone production was decreased by only 50 % in acetaldehyde TPSR with the addition of CO, the combined effect of low surface intermediate concentrations and less basic sites are responsible for the marked decrease in acetone production during ethanol TPSR when CO (5 %) is present in the He carrier stream.

4.2.3. Methanol TPSR

Propionaldehyde or 1-propanol are likely precursors to isobutyraldehyde and isobutanol during CO/H_2 reactions. Propionaldehyde and 1-propanol can form via aldol condensation between C_2 and C_1 oxygenates. In order to study the cross-coupling reactions between C_2 and C_1 oxygenates, we have undertaken a TPSR study of C_1 oxygenates such as CH_3OH on K-promoted $Cu/MgO/CeO_2$ catalysts.

The TPSR of methanol yielded mainly a broad unreacted methanol peak (Fig. 27), indicating a broad range in the strength of adsorption sites. Dimethyl ether (DME), was evolved at 120 °C from methanol dehydration reactions. DME formation was also observed on $K\text{-}Cu/MgO/CeO_2$. This reaction is most likely to occur on sites associated with coordinately unsaturated Ce^{4+} ions, which exhibit Lewis acidity [34]. This explanation is supported by the absence of dimethyl ether in the product of CH_3OH TPSR on Cu/MgO. Small amounts of H_2, H_2O and carbon oxides were also observed on MgO/CeO_2. H_2 production was higher on $K\text{-}Cu/MgO/CeO_2$ and Cu/MgO than on MgO/CeO_2, suggesting that copper is involved in methanol dehydrogenation and H_2

desorption. Interestingly, a hydrogen peak appeared at 260 °C, which was absent during ethanol TPSR. The only difference between ethanol and methanol is that the dehydrogenation product (acetaldehyde) of the former does not undergo subsequent dehydrogenation reactions to produce H_2, while the formaldehyde formed by methanol dehydrogenation reacts further on the surface to generate H_2 and CO On Cu/MgO, large amount of CO was also formed, though it evolved at temperature about 10 °C higher than H_2. On K-Cu/MgO/CeO_2, CO production decreased, while CO_2 increased compared to that on Cu/MgO. Some of the high-temperature CO_2 products may be formed by CO oxidation using lattice oxygen from CeO_2. The presence of formate on K-Cu/MgO/CeO_2 may also lead to the formation of CO_2 and H_2. It should be pointed out that no gas-phase formaldehyde was observed on these catalysts. Formaldehyde, once formed, is likely to decompose immediately to H_2 and carbon oxides before detection.

Task 5: Bench Scale Testing at Air Products and Chemicals

Activities during this reporting period have included meetings between the UCB program manager and Dr. Bernard Toseland at Berkeley.

REFERENCES:

1. C.R., Apesteguia, S.L., Soled, S., Miseo, S., *U.S. Patent No. 5,387,570.* Issued Feb. 7, 1995 to Exxon Research & Engineering Co., Florham Pk., N.J.
2. C. Lamonier, A. Bennani, A. D'uysser, A. Aboukais, and G. Wrobel *J. Chem. Soc., Faraday Trans.*, **92(1)**, 131-136 (1996)
3. T.E. Holt, A.D. Logan, S. Chakraborti, and A.K. Dayte *Applied Catal.* **34,** 199-213 (1987).
4. L. Volpe, and M. Boudart *Catal. Rev. -Sci. Eng.*, **27(4)**, 515-538 (1985).
5. M. Ueshima, and Y. Shimasaki *Catal. Lett.* **15,** 405-411 (1992)
6. D.J. Driscoll, W. Martir, J.-X. Wang, and J. H. Lunsford, *J. Am. Chem. Soc.*, **107,** 58-63 (1985)
7. J.H. Lunsford, M.D. Cisneros, P.G. Hinson, Y. Tong, and H. Zhang, *Faraday Discuss. Chem. Soc.*, **87**, 1-10 (1989)
8. J.C. Slaa, J.G. van Ommmen and J.R.H. Ross, *Catal. Today* **15,** 129-148 (1992).
9. A. Sofianos, *Catal. Today* **15,** 149-175 (1992).
10. G.A. Vedage, P.B. Himelfarb, G.W. Simmons and K. Klier, *ACS Symposium Series* **279,** 295 (1985).
11. D.J. Elliot and F. Penella, *J. Catal.* **119,** 359 (1989).
12. K. Kawamoto and Y. Nishimura, *Bull. Chem. Soc. Japan* **44** 819-825 (1971).
13. K. Takeshita, S. Nakamura and K. Kawamoto, *Bull. Chem. Soc. Japan* **59(9),** 2622-2627 (1978).
14. I.E. Wachs and R.J. Madix, *Appl. Surf. Sci.* **1,** 303 (1978).
15. M. Bowker and R.J. Madix *Surf. Sci.* **116**, 549-572 (1982)
16. M.J. Chung, S.H. Han, K.Y. Park and S.K. Ihm, *J. Molec. Catal.* **79,** 335-345 (1993).

17. M. Bowker, H. Houghton and K.C. Waugh *J. Chem. Soc., Faraday Trans. 1*, **78**, 2573-2582 (1982)
18. J.M. Vohs and M.A. Barteau *Surf. Sci.* **221**, 590-608 (1989)
19. S. Halawy and M.A. Mohamed, *J. Molec. Catal. A:Chemical* **98,** L63-L68 (1995).
20. X. Xu, E. B. M. Doesburg, J. J. F. Scholten, *Catal. Today* **2**, 125-170 (1987).
21. J.G.,Nunan, C.E., Bogdan, K., Klier, K.J., Smith, C.-W., Young, and R.G. Herman, *J. Catal.* **113** (1988) 410.
22. G. Zhang, H. Hattori, K. Tanabe, *Bull. Chem. Soc. Jpn.* **62**, 2070-2072 (1989).
23. G.A., Vedage, P.B., Himelfarb, G.W., Simmons, and K. Klier, *ACS Symp. Ser.* **279** (1985) 295.
24. W. Ueda, T. Ohshida, T. Kuwabara, Y. Morikawa, *Catal. Lett.* **12**, 97-104 (1992).
25. E. Iglesia, and M. Boudart *J. Catal.* **81**, 204-213 (1983)
26. K. Narita, N. Takeyawa, H. Kobayashi, and I. Toyoshima *React. Kinet. Catal. Lett.* **19** (1982)
27. J.J.F. Scholten, and J.A. Konvalinka *Trans. Faraday Soc.* **65**, 2465 (1969)
28. G.R. Sheffer, and T.S. King *J. Catal.* **115**, 376-387 (1989).
29. P.-J. Chu, B.C. Gerstein, G.R. Sheffer, and T.S. King *J. Catal.* **115**, 194-204 (1989)
30. G. R. Sheffer, and T.S. King *J. Catal.* **116**, 488-497 (1989)
31. L.L. Murrell, S.J. Tauster, and D. R. Anderson *Catalysis and Automobile Pollution Control II*, Elsevier, Amsterdam, 1991]
32. J. Soria *Solid State Ionics*, **63-65**, 755-761 (1993)
33. H. Tsuji, F. Yagi, H. Hattori, and H. Kita *J. Catal*, **148**, 759-770 (1994)
34. C. Li, K. Domen, K. Maruya, and T. Onishi *J. Catal.* **125**, 445-455 (1990)
35. J.D. Roberts and M.C. Caserio *Modern Organic Chemistry*, P373
36. F. Gonzalez, G. Munuera and J.A. Prieto *J. Chem. Soc., Faraday Trans.* **I, 74**, 1517 (1978)
37. M. Bowker and R.J. Madix *Appl. Surf. Sci.* **8**, 299-317 (1981)
38. M. Bowker, H. Houghton and K.C. Waugh *J. Catal.* **79**, 431-444 (1983)
39. S.L. Parrott, J.W. Rogers, Jr. and J.M. White Appl. *Surf. Sci.* **1**, 443-454 (1978)

4. PARTICIPATING PROJECT PERSONNEL

Mingting Xu
Postdoctoral Fellow

Marcelo J. L. Gines
Postdoctoral Fellow

Brandy L. Stephens
Graduate Student

Tom Wang
Undergraduate Researcher

Bernard A. Toseland
Sub-Contractor
Air Products and Chemicals

Enrique Iglesia
Principal Investigator

Table 2: Patent [1], CMRU-8, and CMRU-9 Results on K-$Cu_{0.5}Mg_5CeO_x$

	Patent	CMRU-8	CMRU-9
Catalyst	K-$Cu_{0.5}Mg_5CeO_x$	$Cu_{0.5}Mg_5CeO_x$	K-$Cu_{0.5}Mg_5CeO_x$
Mg/Ce	5	5	5
Source		MG3-1b O	MG3-1b O/K
Data File		\1c8-1832.1-9	\1c9-180!.1-9
Charge (g)	3.00	2.98	3.00
T (°C)	320	325	250
P (atm)	50	50	50
GHSV (cm^3(STP)/g cat.h)	1832	1832	1800
H2:CO	1	1	1
CO Conversion	15.5%	5.4%	19.2%
Product Selectivities			
methanol	**57.19**	**87.76**	**96.90**
ethanol	1.87	0.73	0.42
1-propanol	2.64	0	0.12
isopropanol	not reported	0	0
2-butanol	not reported	0	0.07
isobutanol	**10.44**	0	**0.21**
1-butanol	0.28	0	0
1-pentanol	0.68	0	0
2-methyl-1-butanol	1.17	0	0
paraffins	24.31	11.17	2.05
CO2	31.04	15.43	3.55
Σ Selectivities-Sel. CO_2	105	100	100

Table 3: Patent [1] and CMRU-10 Results on K-$Cu_{0.5}Mg_5CeO_x$

	Patent	**CMRU-10**	**CMRU-10**
Catalyst	0.9% K - $Cu_{0.5}Mg_5CeO_x$	3.0% K - $Cu_{0.5}Mg_5CeO_x$	3.0% K - $Cu_{0.5}Mg_5CeO_x$
Mg/Ce	5	5	5
Source		MG3-1b O/K	MG3-1b O/K
Data File		\1cmru-10.4-12	\2cmru-10.1-7
Charge (g)	3.00	3.04	3.04
T (°C)	320	250	250
P (atm)	50	50	50
GHSV (cm^3(STP)/g cat.h)	1832	1776	888
H2:CO	1	1	1
CO Conversion	15.5%	3.3%	6.5%
Product Selectivities			
methanol	**57.19**	**97.5**	**93.2**
ethanol	1.87	0.93	0.69
1-propanol	2.64	0.06	0.22
1-butanol	0.28	0	0
isobutanol	**10.44**	**0.10**	**0.37**
1-pentanol	0.68	0	0
2-methyl-1-butanol	1.17	0	0
paraffins	24.31	1.31	5.13
CO2	31.04	14.52	8.34
Σ Selectivities-Sel. CO_2	105	100	100

Table 4: Patent [1], CMRU-12, and CMRU-13 Results at T = 320 °C

	Patent	CMRU-12	CMRU-13
Catalyst	0.9% K - $Cu_{0.5}Mg_5CeO_x$	0.9% K - $Cu_{0.5}Mg_5CeO_x$	0.9% K - $Cu_{0.5}Mg_5CeO_x$
BET S.A. (m2/g)	not reported	162	190
Mg/Ce	5	5	5
Source		MG3-10b O/K	MG3-10 O/K
		\3cmru12.1-9	\3cmru13.12-9
Charge (g)	3.00	3.01	4.32
T (°C)	320	320	321
P (atm)	50	50	50
GHSV (cm^3(STP)/g cat.h)	1832	1794	1813
H2:CO	1	1	1
CO Conversion	15.5%	14.4%	20.8%
Product Selectivities			
methanol	**57.19**	**73.72**	**65.05**
ethanol	1.87	0.30	0.36
1-propanol	2.64	0.49	2.95
isopropanol	not reported	0.82	0.98
2-butanol	not reported	0.45	0.23
isobutanol	**10.44**	**7.85**	**12.96**
1-butanol	0.28	0.01	0.32
1-pentanol	0.68	0.13	0.16
2-methyl-1-butanol	1.17	0.51	1.04
CO2	31.04	25.85	12.29
DME	1.16	1.86	1.33
acetaldehyde	not reported	not detected	0.24
CH4	**11.52**	**6.86**	**3.68**
C2+ paraffins	12.79	2.67	0.52
MeOH/i-BuOH	5.5	9.4	5.0
Alc/HCs	2.94	9.26	22.7

Table 5: Patent [1], CMRU-12, and CMRU-13 Results at T > 330 °C

	Patent	CMRU-12	CMRU-12	CMRU-13
Catalyst	0.9% K - $Cu_{0.5}Mg_5CeO_x$	0.9% K - $Cu_{0.5}Mg_5CeO_x$	0.9% K - $Cu_{0.5}Mg_5CeO_x$	0.9% K - $Cu_{0.5}Mg_5CeO_x$
BET S.A. (m^2/g)	not reported	162	162	190
Mg/Ce	5	5	5	5
Source		MG3-10b O/K	MG3-10b O/K	MG3-10 O/K
		\4cmru12	\6cmru12	\4cmru13b
Charge (g)	3.00	3.01	3.01	4.32
T (°C)	**360**	**341**	**362**	**331**
P (atm)	50	50	50	50
GHSV (cm^3(STP)/g cat.h)	1832	1794	1794	1813
H2:CO	1	1	1	1
CO Conversion	19.0%	8.0%	4.1%	6.8%
Product Selectivities				
methanol	26.27	72.44	57.08	41.47
isobutanol	10.94	14.80	17.40	26.65
paraffins	60.1	4.07	10.58	6.16
CO_2	not reported	29.44	54.62	23.69
Σ Selectivities-Sel. to CO_2	100	100	100	100
MeOH/i-BuOH	2.4	5.0	3.3	1.6
Alc/HCs	0.66	26.2	7.8	14.7

Table 6: CMRU-13 (MG3-10 O/K) and CMRU-14 (MG3-10 O/Cs) Results

	CMRU-13	CMRU-14
Catalyst	0.9% K-$Cu_{0.5}Mg_5CeO_x$	0.9% Cs-$Cu_{0.5}Mg_5CeO_x$
BET S.A. (m^2/g)	190	143
Mg toCe ratio	5	5
Source	MG3-10 O/K	MG3-10 O/Cs
	\3cmru13.12-9	\4cmru14.1-9
Charge (g)	4.32	3.21
T (°C)	321	320
P (atm)	50	50
GHSV (cm^3/g cat.h)	1813	1862
H2:CO	1	1
CO Conversion	20.8%	9.0%
Product Selectivities		
methanol	**65.05**	**62.12**
ethanol	0.36	1.11
1-propanol	2.95	5.02
isopropanol	0.98	2.99
2-butanol	0.23	0.32
isobutanol	**12.96**	**11.58**
1-butanol	0.32	0.12
1-pentanol	0.16	0.56
2-methyl-1-butanol	1.04	1.39
CO2	12.29	22.39
DME	1.33	2.44
acetaldehyde	0.24	0.43
CH4	3.68	2.33
C2+ paraffins	0.52	0.28
Σ Selectivities-Sel. to CO_2	100	100
MeOH/i-BuOH	5.0	5.4
Alc/HCs	22.7	31.9

Table 9: CMRU-15 (MG3-11 O/K) and CMRU-16 (MG3-11 O) Results

	CMRU-15	CMRU-16
Catalyst	0.9% K - $Cu_{0.5}Mg_5CeO_x$	$Cu_{0.5}Mg_5CeO_x$
BET S.A. (m^2/g)	56	93
Mg toCe ratio	5	5
Source	MG3-11 O/K	MG3-11 O
	\1gc	\1gc8co2
Charge (g)	2.95	3.21
T (°C)	593	593
P (atm)	44	44
GHSV (cm^3(STP)/g cat.h)	6100	5000
H2:CO	1	1
CO Conversion	2.3%	3.2%
Product Selectivities		
methanol	**67.78**	**80.07**
ethanol	3.56	1.91
1-propanol	3.11	2.00
isopropanol	0.93	0.53
2-butanol	0.52	0
isobutanol	**10.22**	**2.77**
1-butanol	0.00	0.31
1-pentanol	0.00	0.11
2-methyl-1-butanol	0.12	0
CO2	16.92	8.70
DME	1.85	1.16
acetaldehyde	0.05	0
CH4	3.35	3.68
C2+ paraffins	0.48	0.78
Σ Selectivities-Sel. to CO_2	100	100
MeOH/i-BuOH	8.5	29.1
Alc/HCs	10.8	20.2

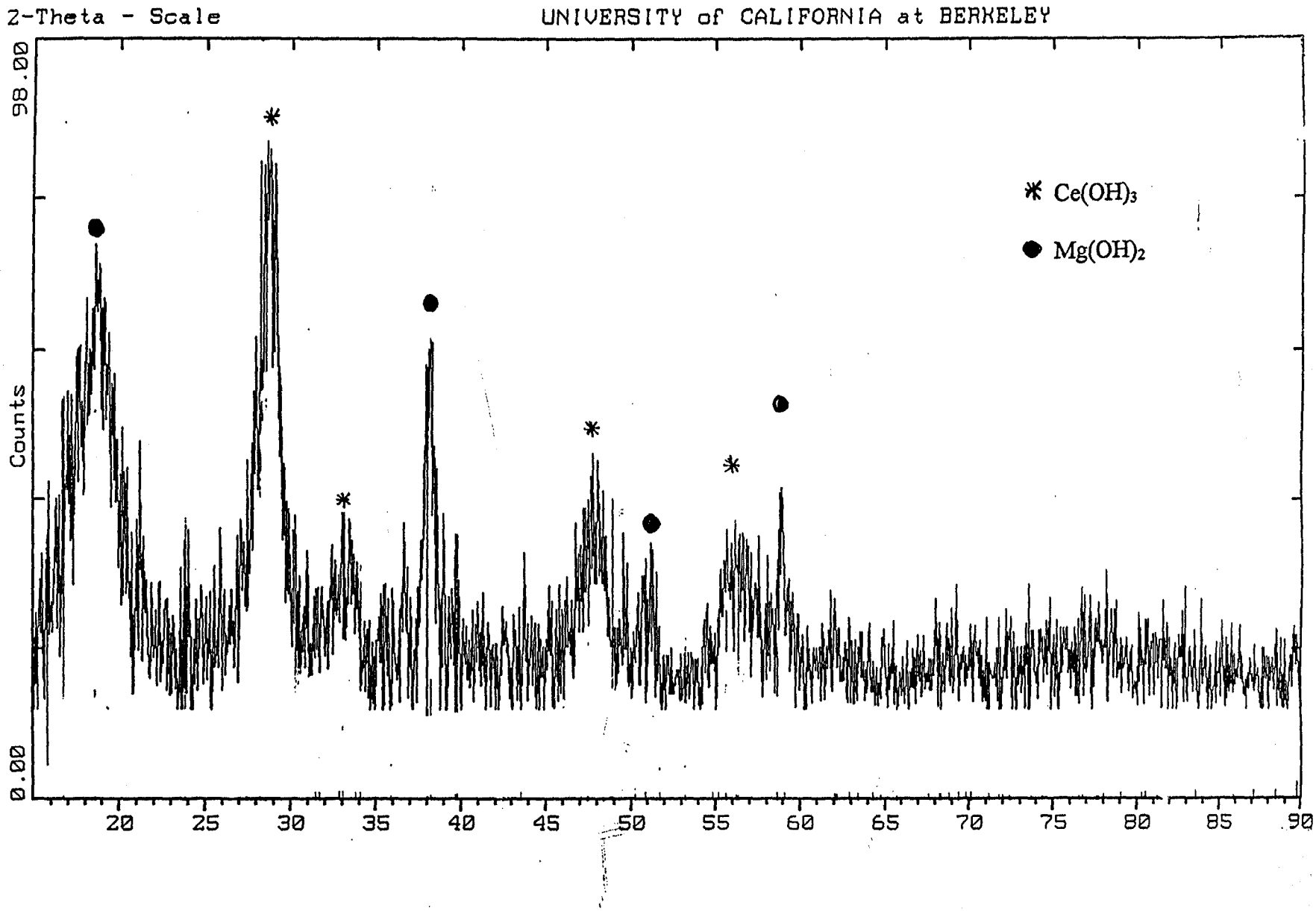

Figure 1: XRD pattern of Cu/Mg/Ce oxide precursor.

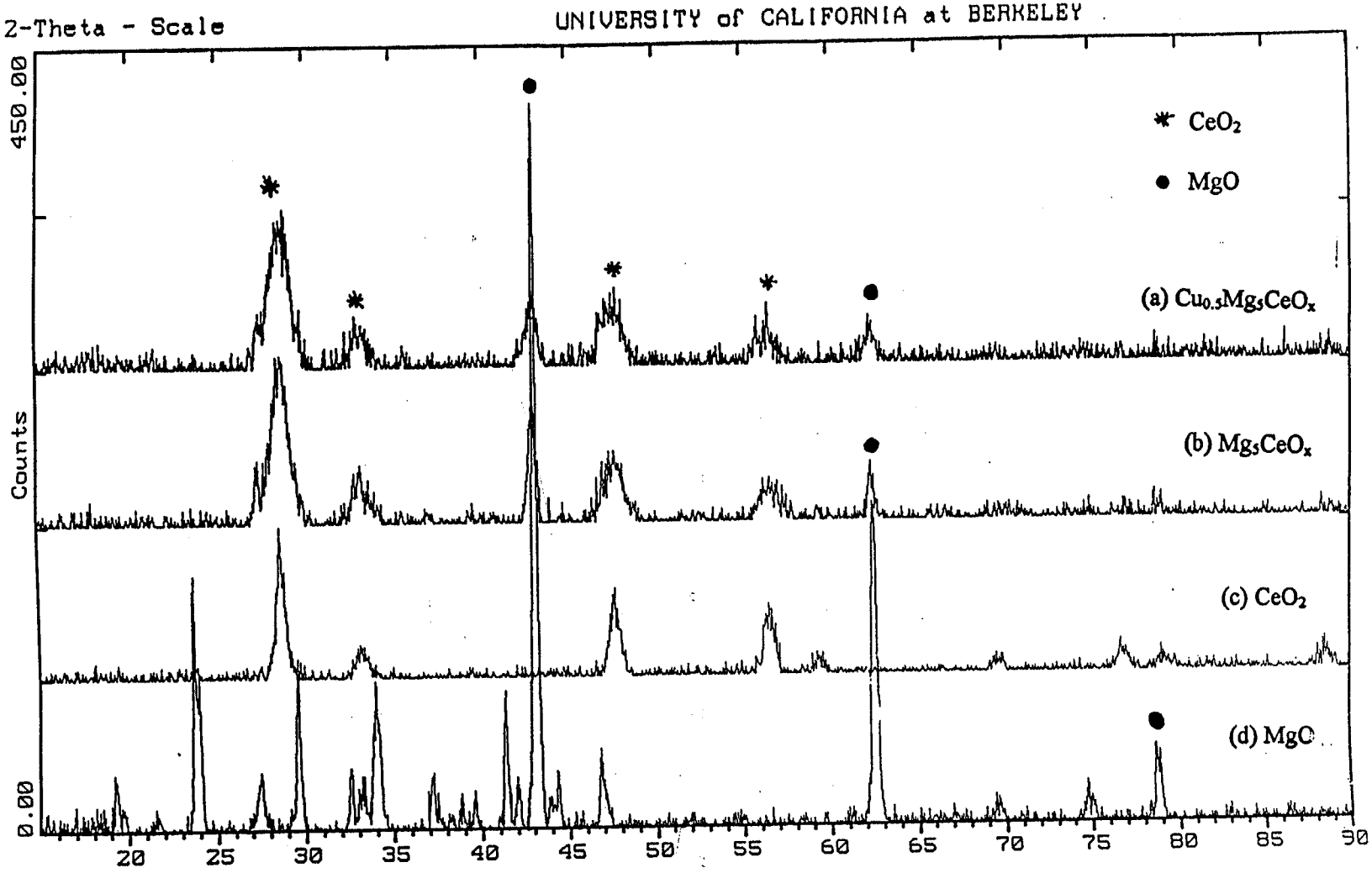

Figure 2: XRD patterns of Cu/Mg/Ce mixed oxides.

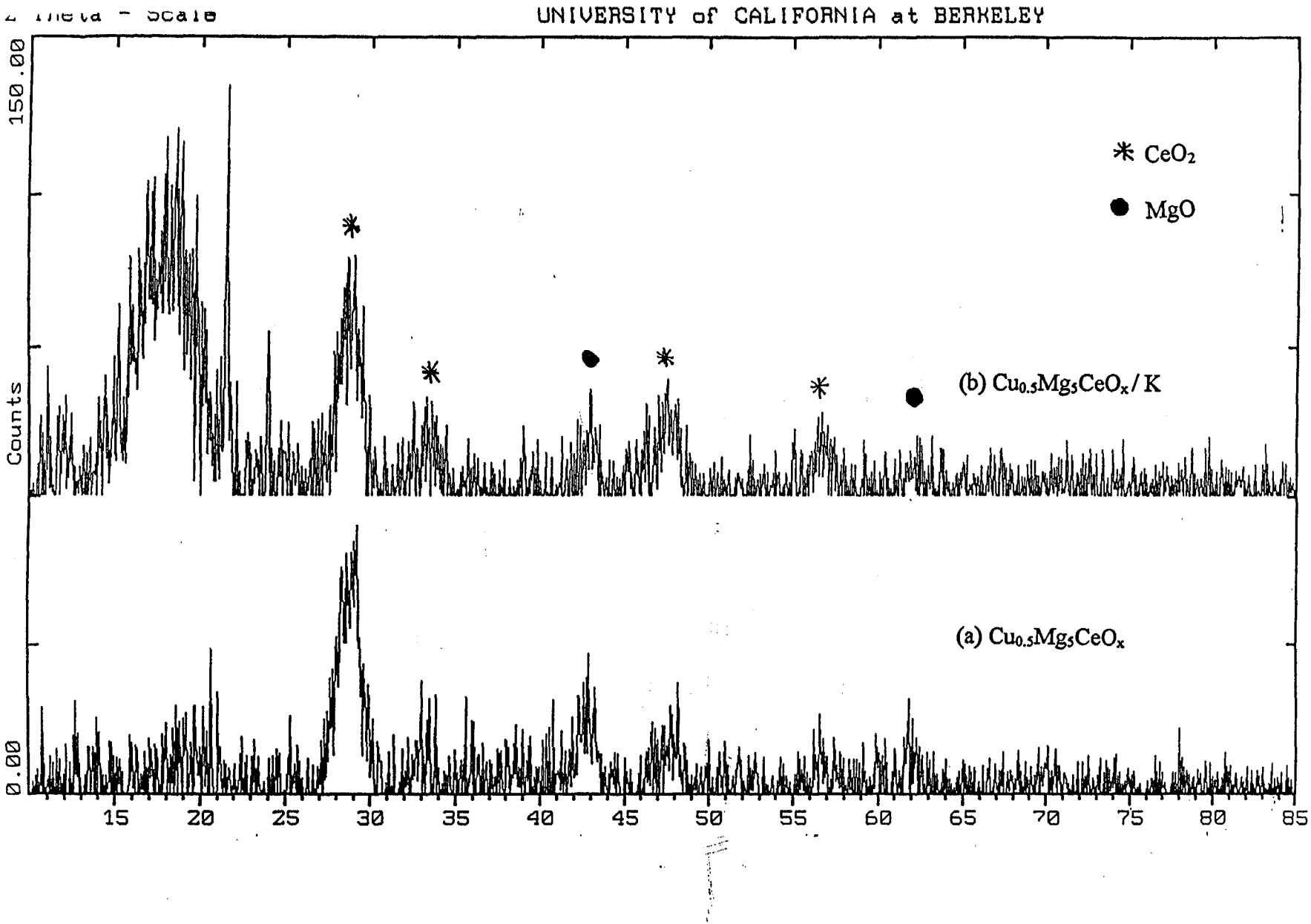

Figure3: XRD pattern of Cu/Mg/Ce oxides. *(a)* Unpromoted catalyst, and *(b)* potassium promoted catalyst.

Fig. 4. Methanol and ethanol turnovers as a function of contact time on Cu/ZnO

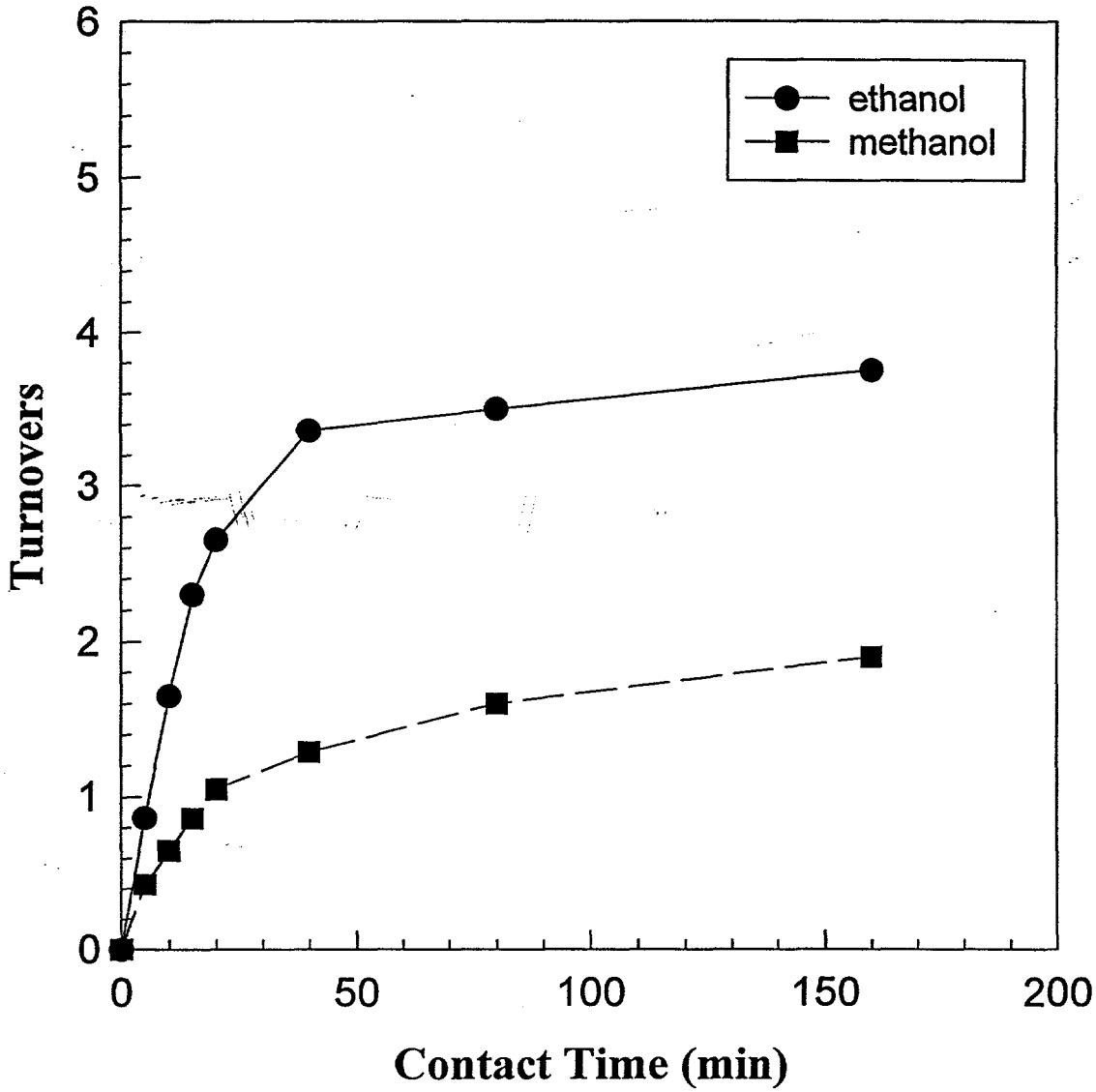

Fig. 5. Product selectivity with respect to ethanol conversion on Cu/ZnO

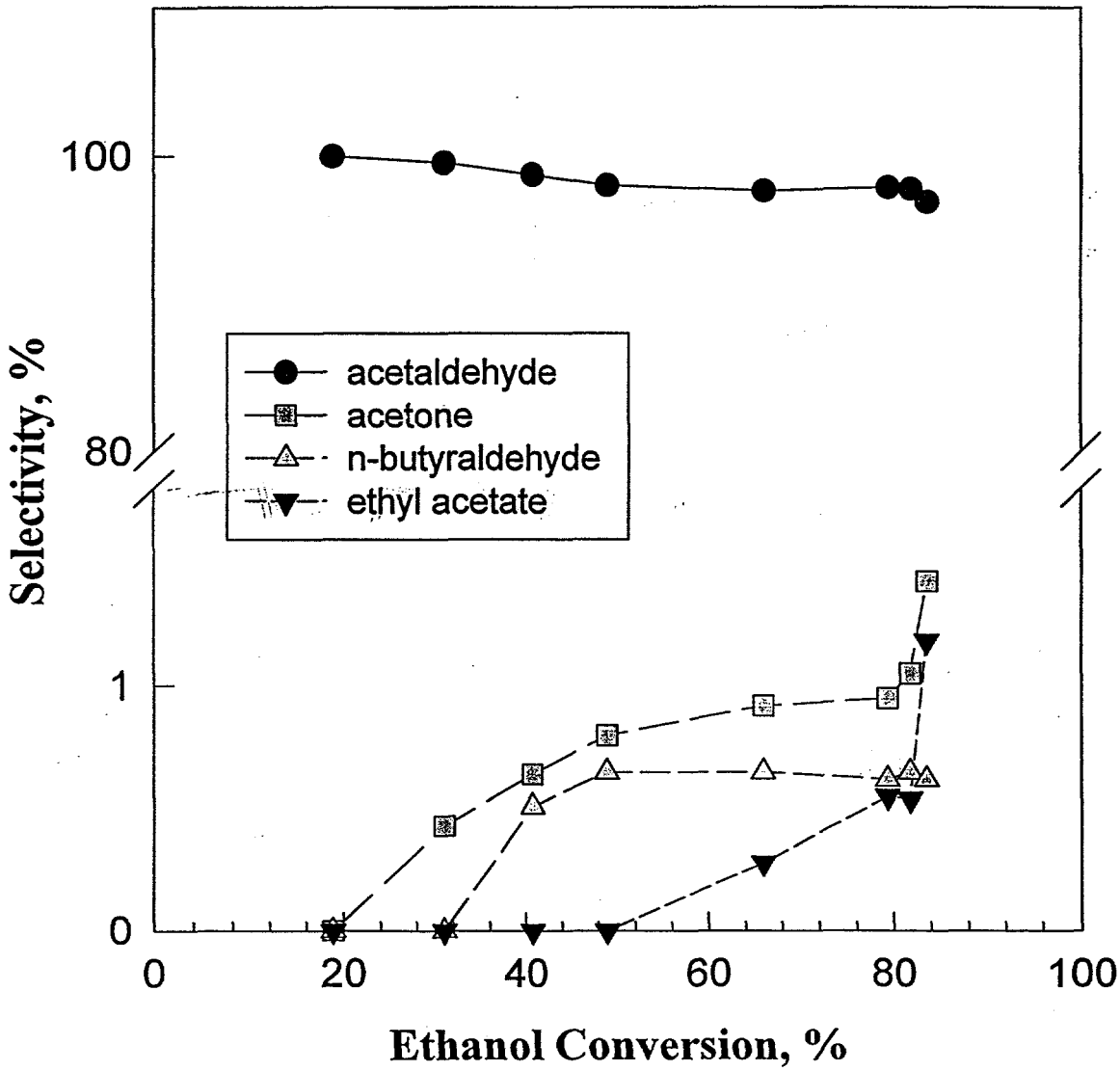

Fig. 6. Ethanol turnovers as a function of time on Cu/ZnO

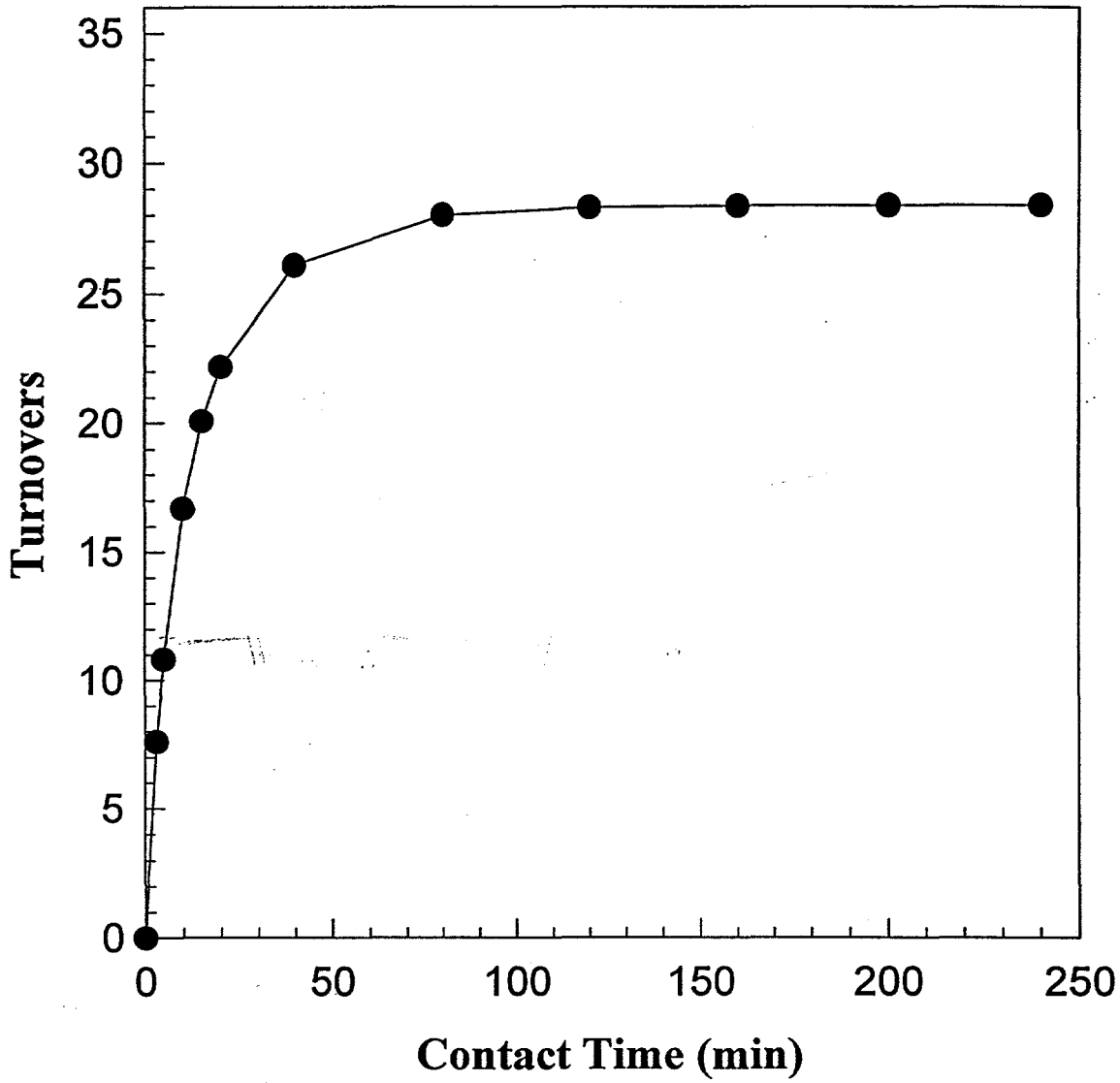

Fig. 7. products selectivity as a function of contact time on Cu/ZnO

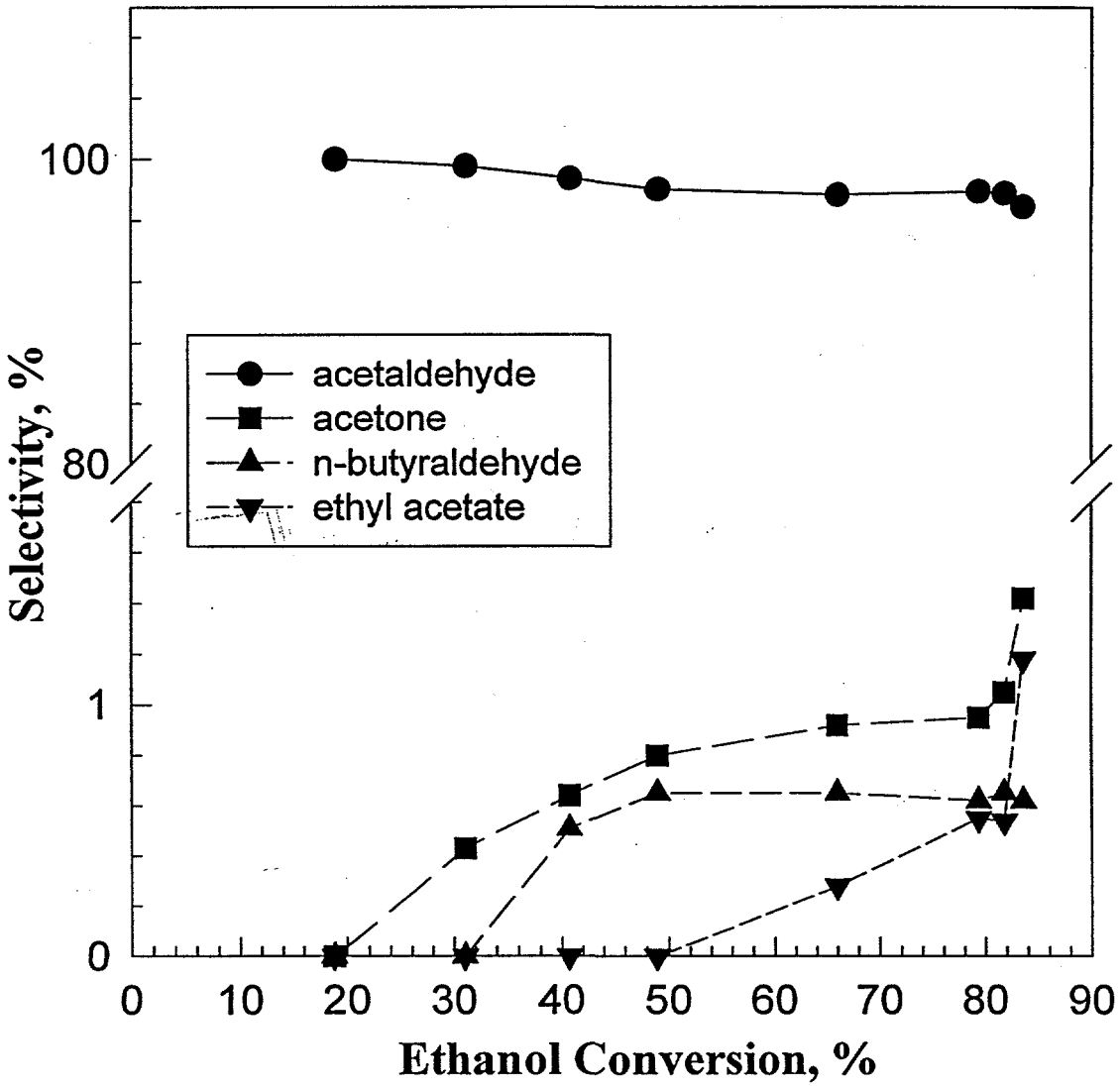

Fig. 8. Ethanol conversion as a function of contact time on Mg_5CeO_x

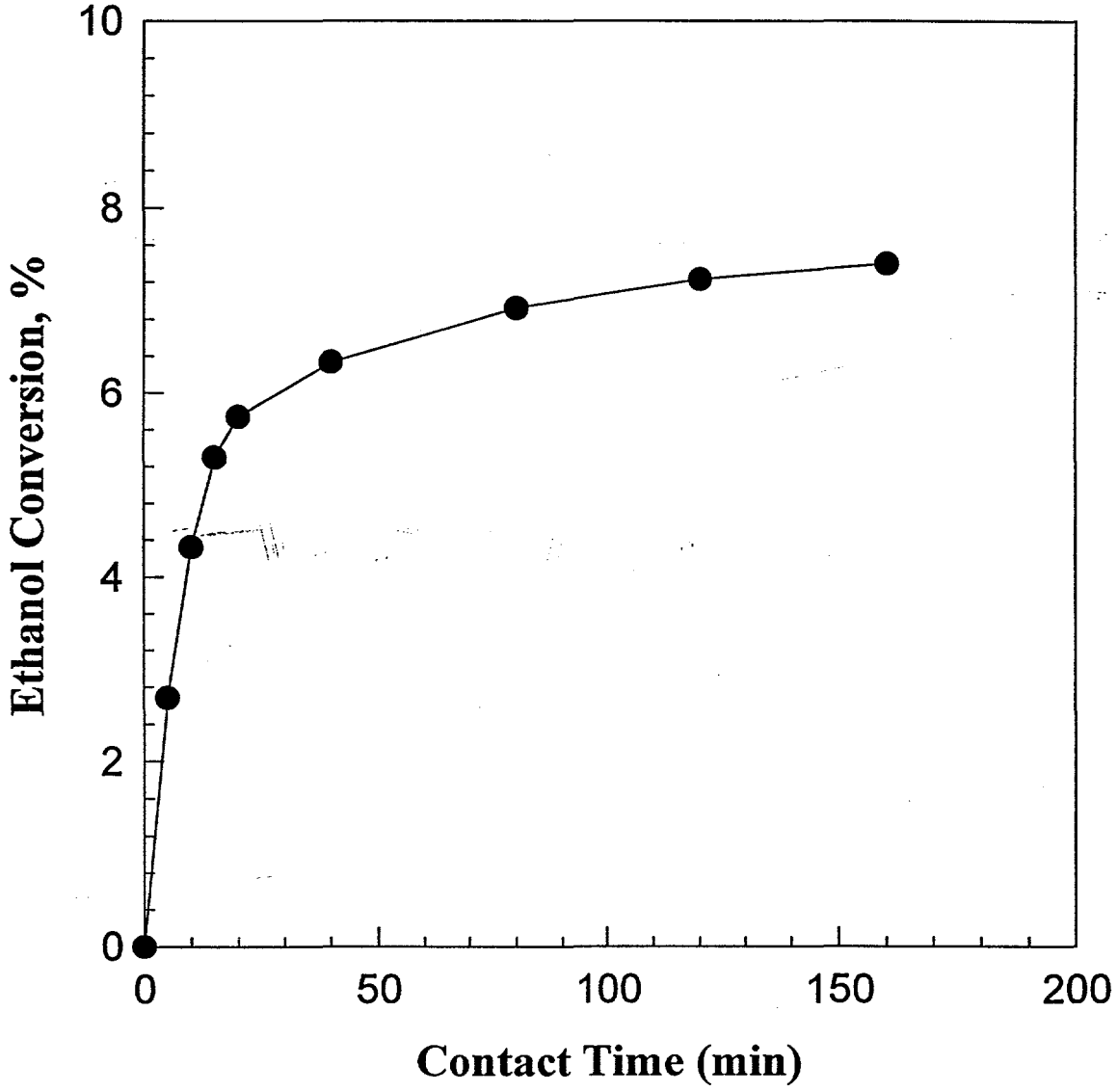

Fig. 9. products distribution as a function of time on Mg_5CeO_x.

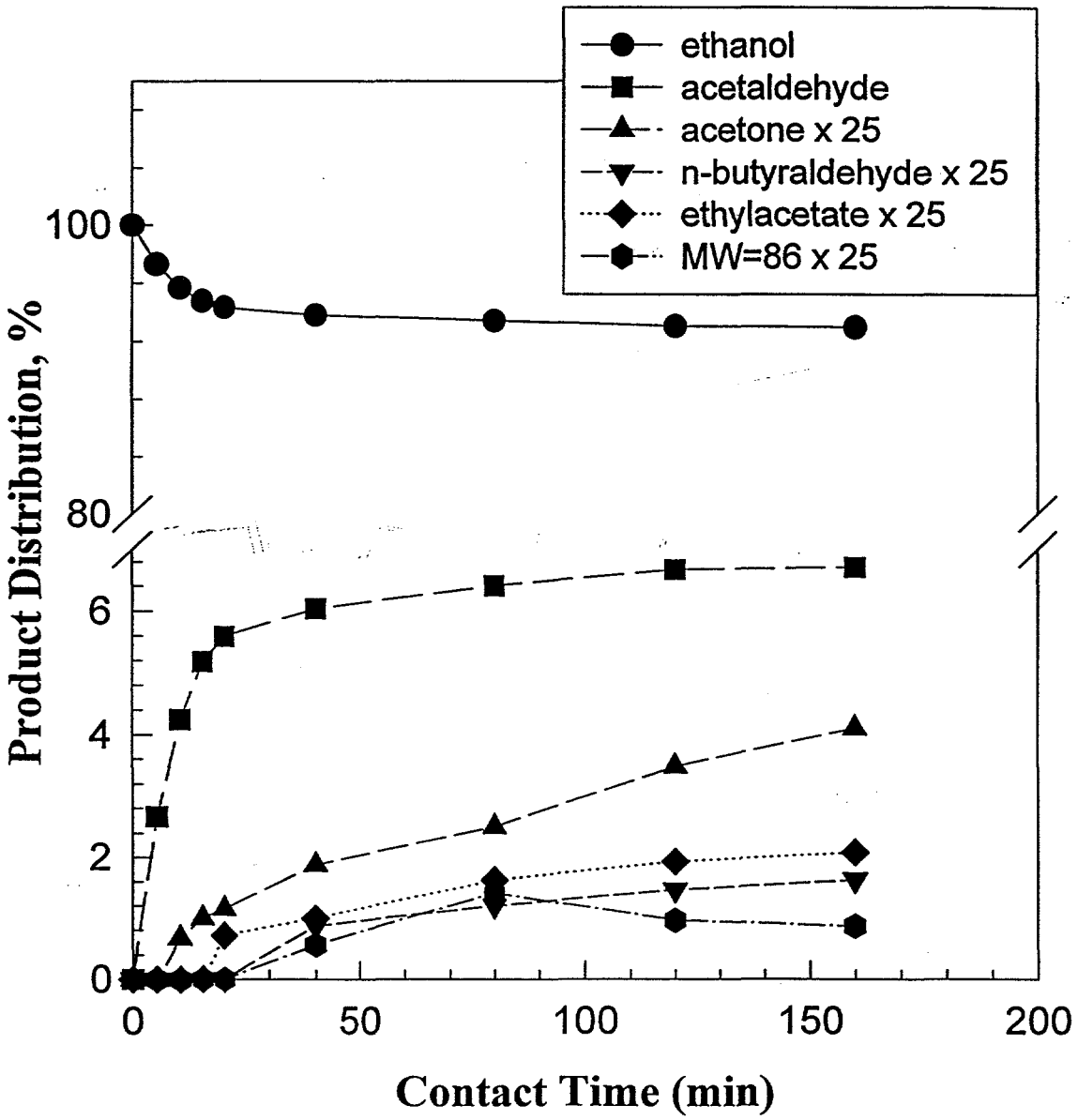

Fig. 10. Ethanol turnovers as a function of time on $Cu_{0.5}Mg_5CeO_x$

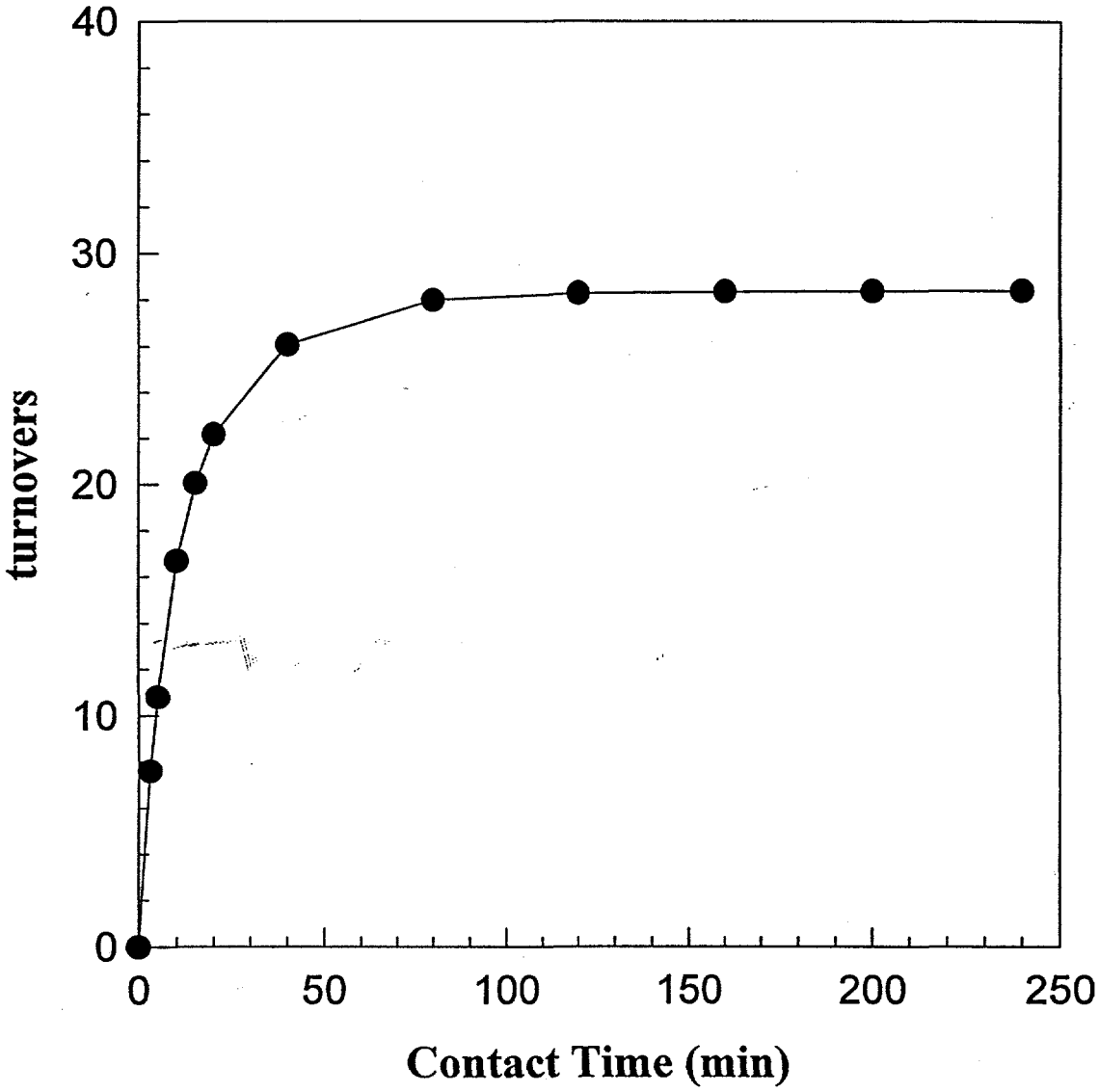

Fig. 11. Ethanol turnovers as a function of time on $Cu_{0.5}Mg_5CeO_X/K$ (1 wt %)

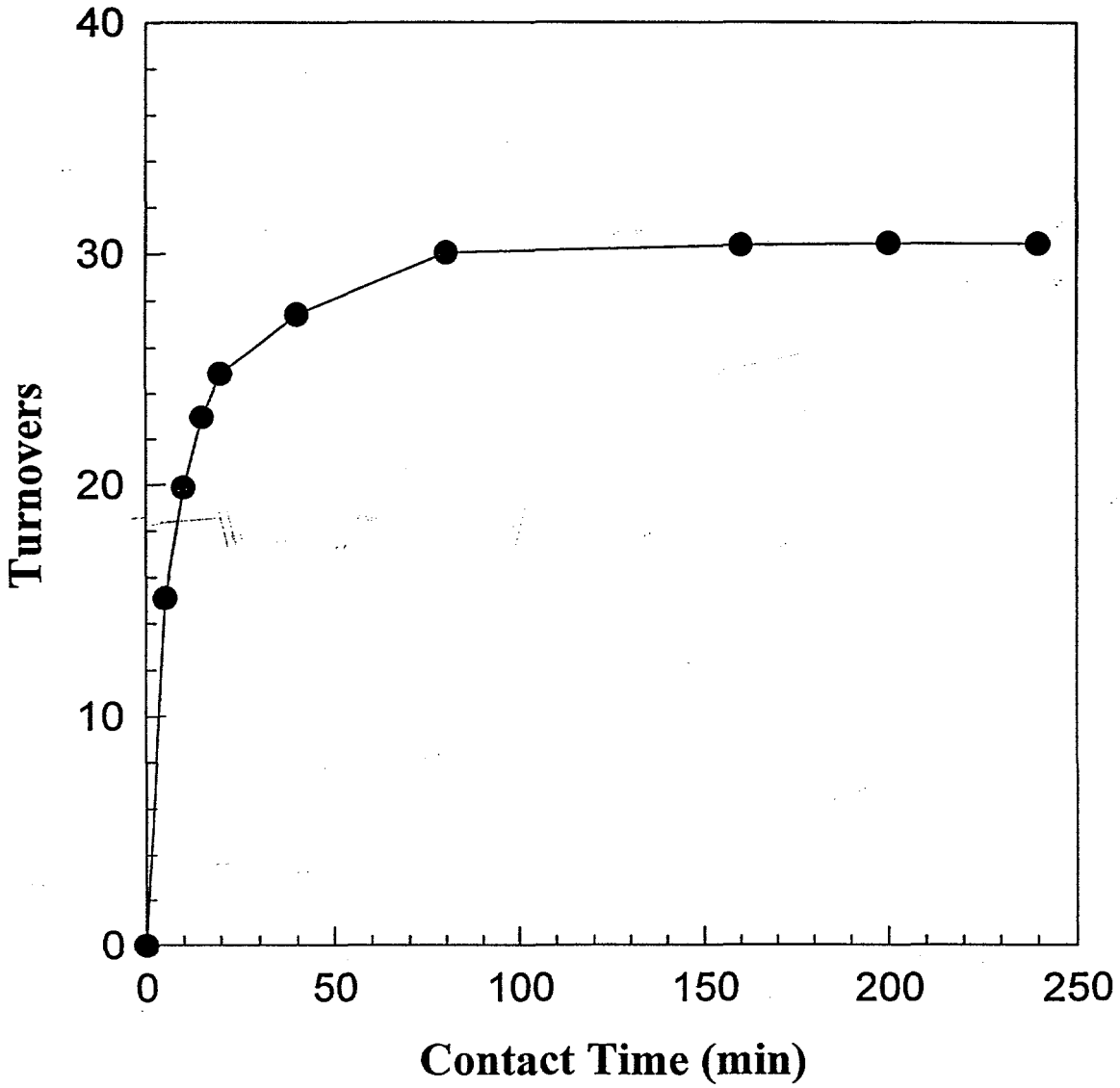

Fig. 12. Product selectivity vs. ethanol conversion$Cu_{0.5}Mg_5CeO_x$

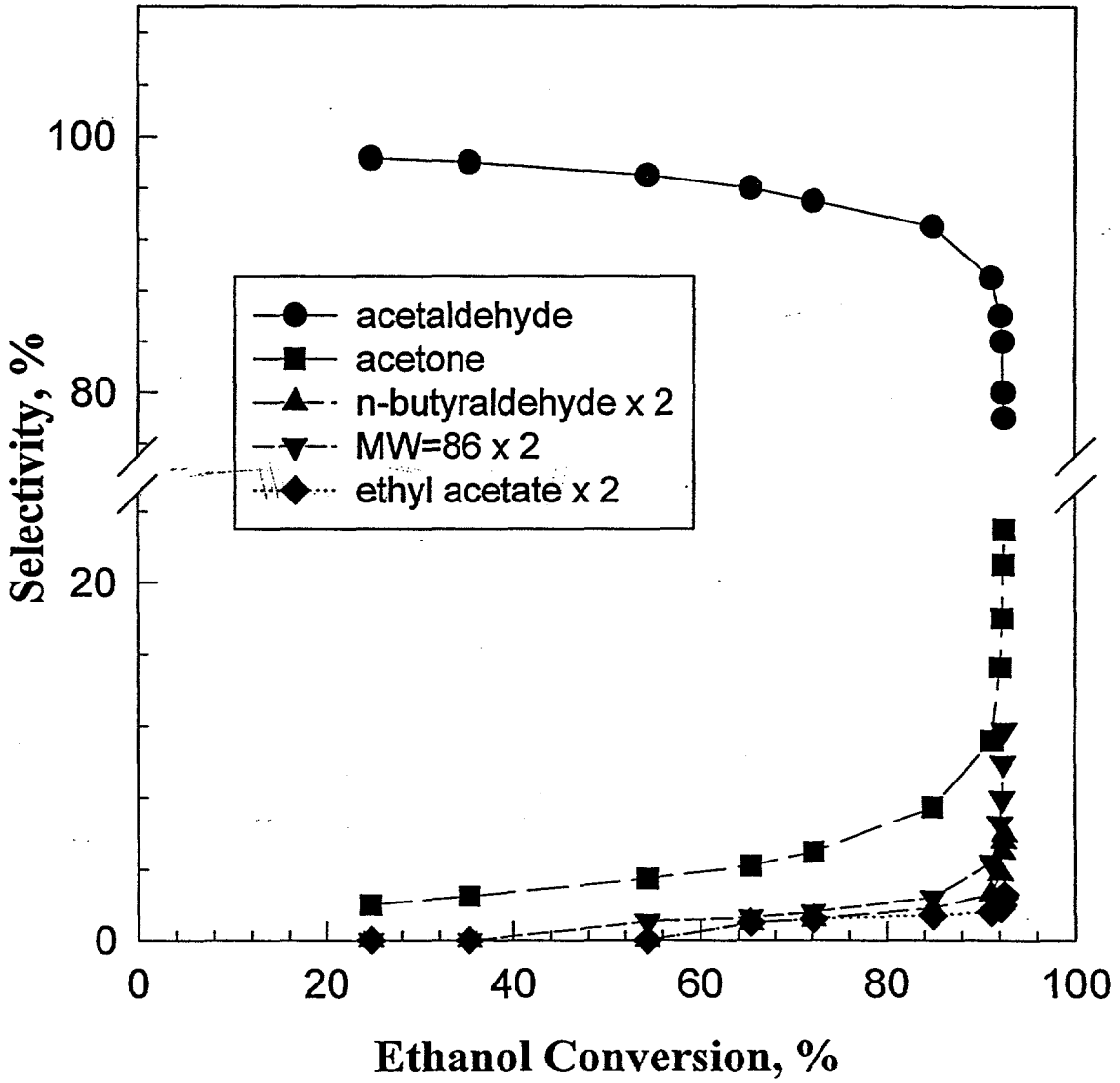

Fig. 13. Product selectivity vs. ethanol conversion on $Cu_{0.5}Mg_5CeO_x/K$ (1 wt %)

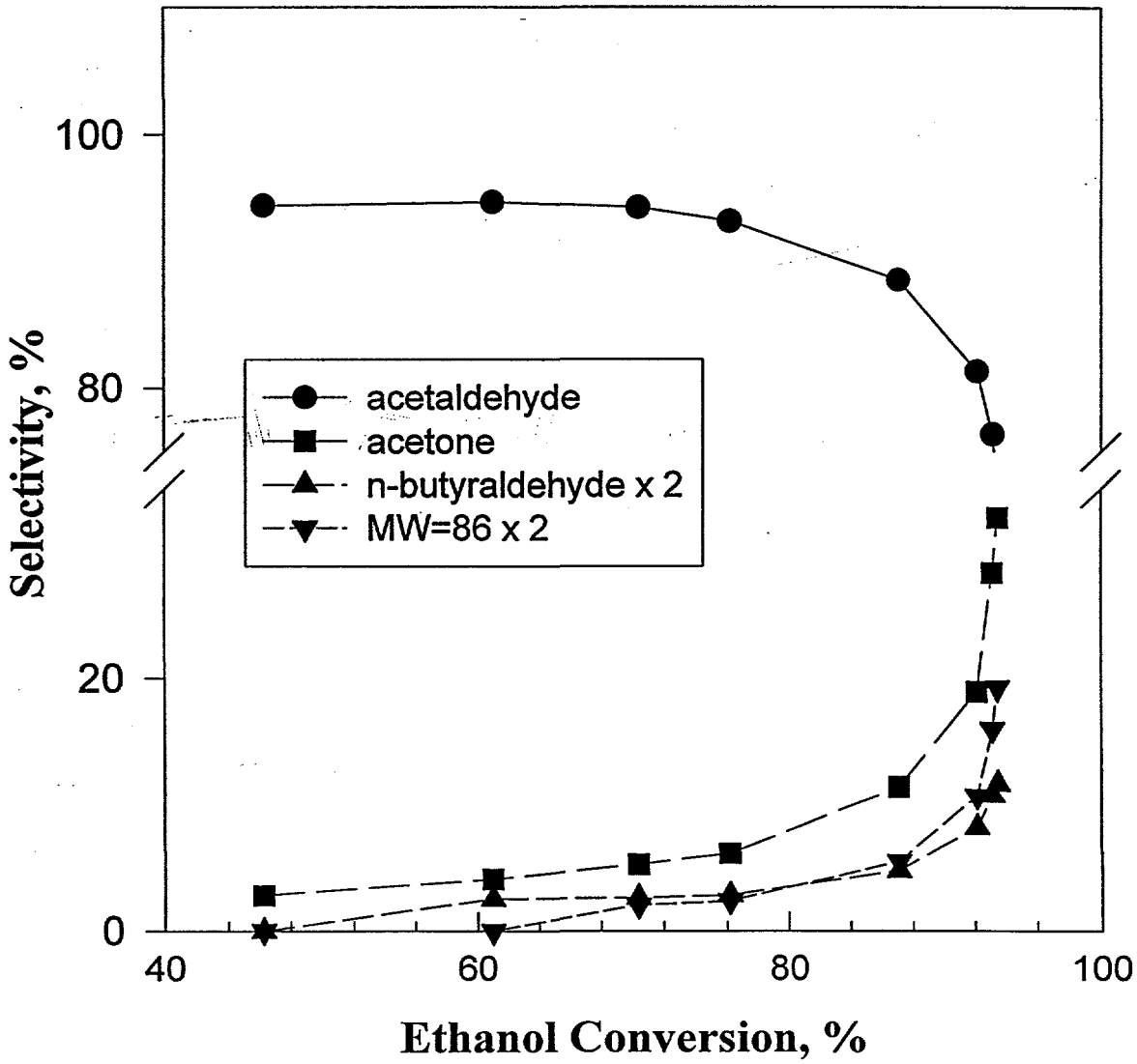

Fig. 14. Products distribution as a function of time on $Cu_{0.5}Mg_5CeO_x$

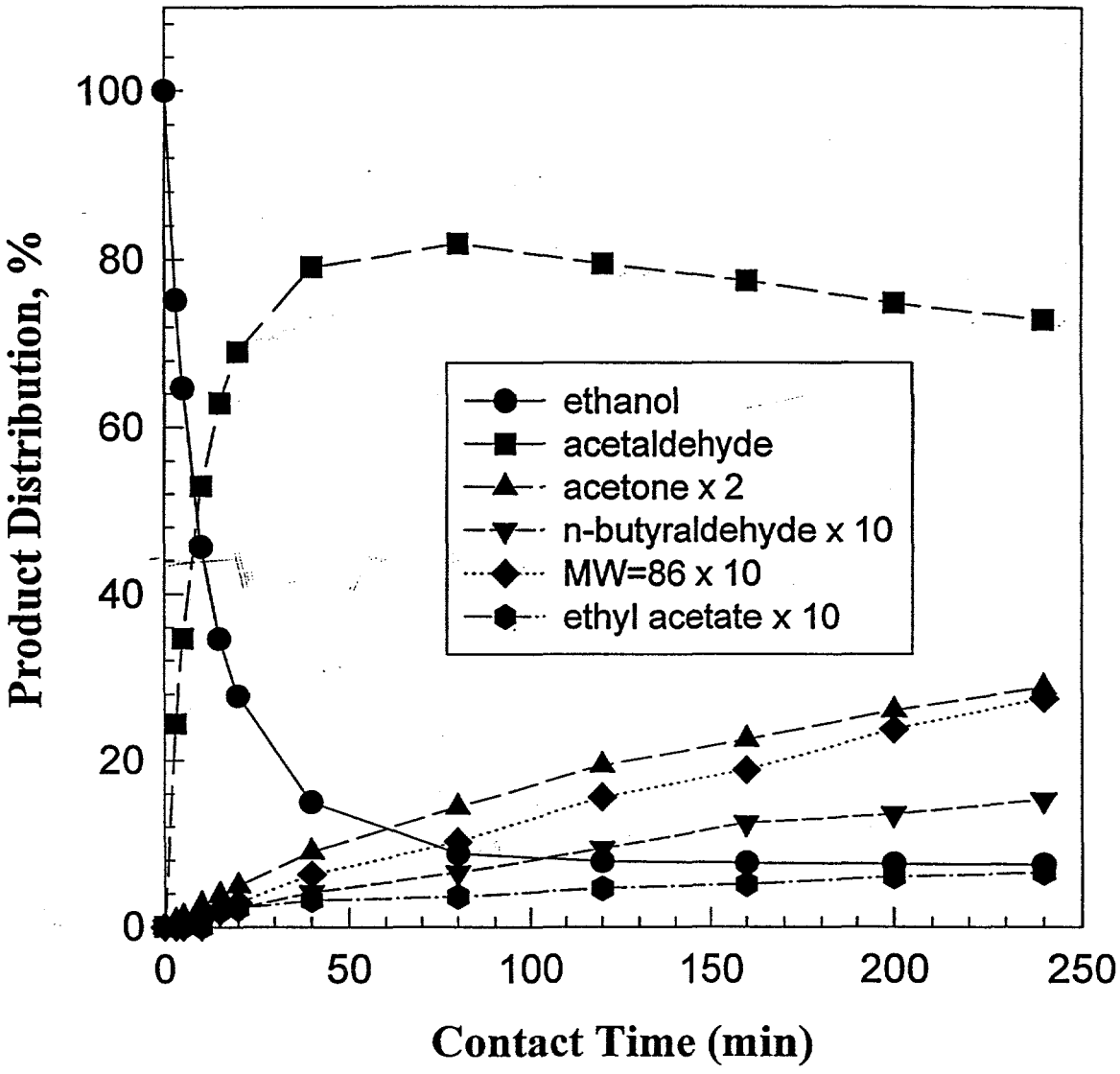

Fig. 15. Product distribution as a function of time on $Cu_{0.5}Mg_5CeO_x/K$ (1wt %)

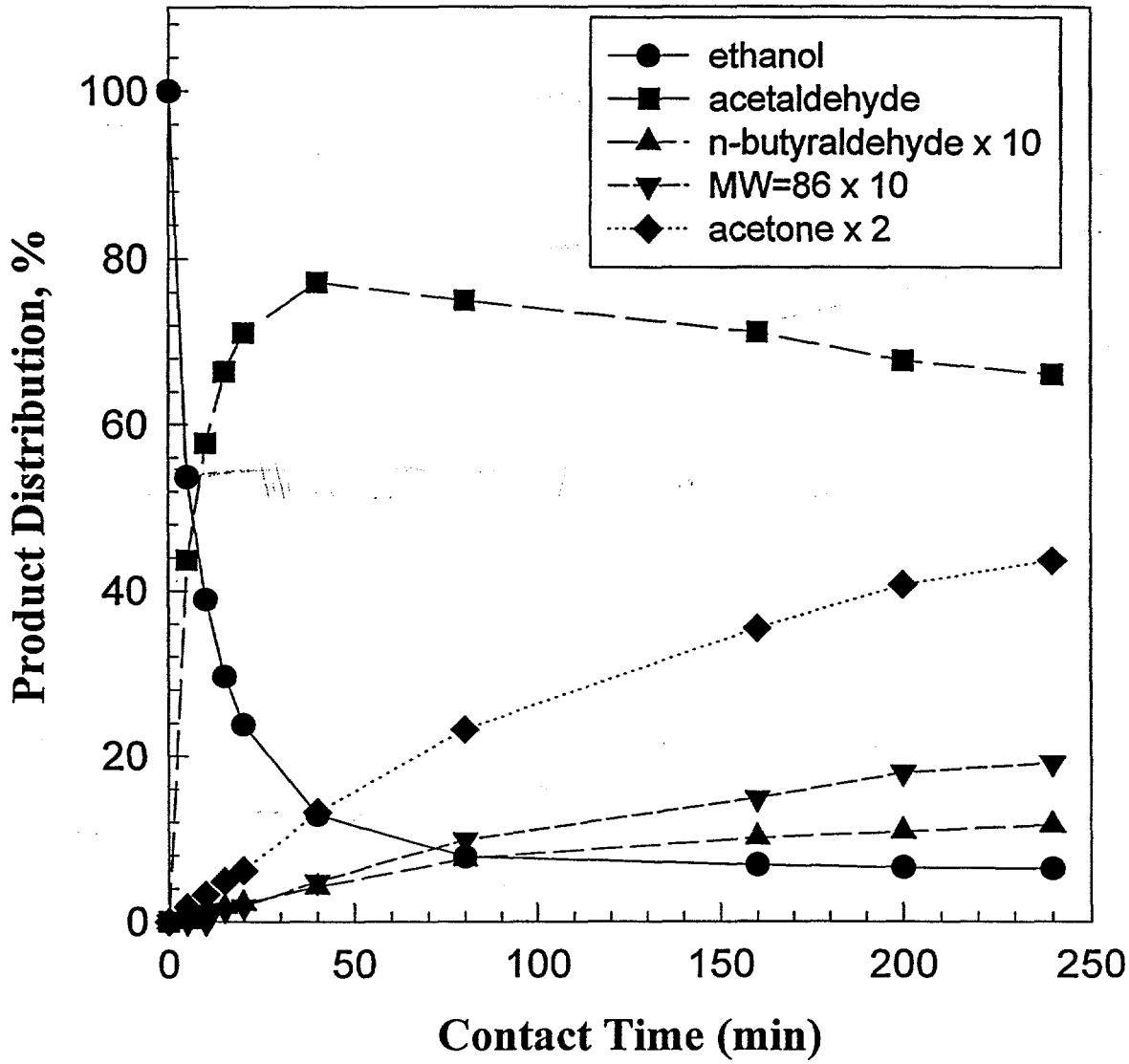

Fig. 16. CO Conversion vs. Reciprocal Space Velocity

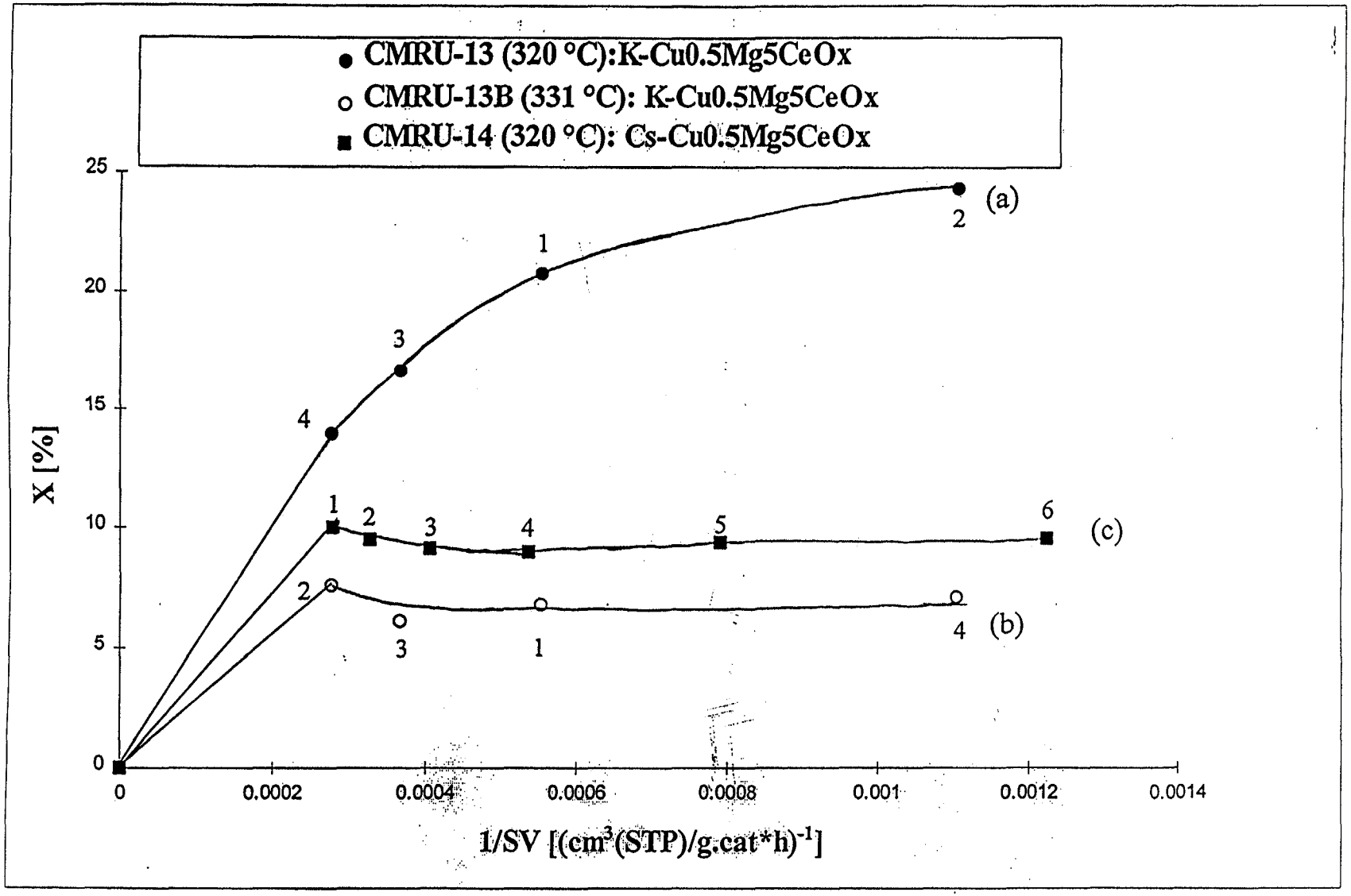

Numbers on plot denote order in which experiment was performed

Fig. 17. Product Selectivities vs. Space Velocity

CMRU-13: K-$Cu_{0.5}Mg_5CeO_x$ (MG3-10 O/K)

T = 320 °C, P = 750 psi, H_2/CO = 1

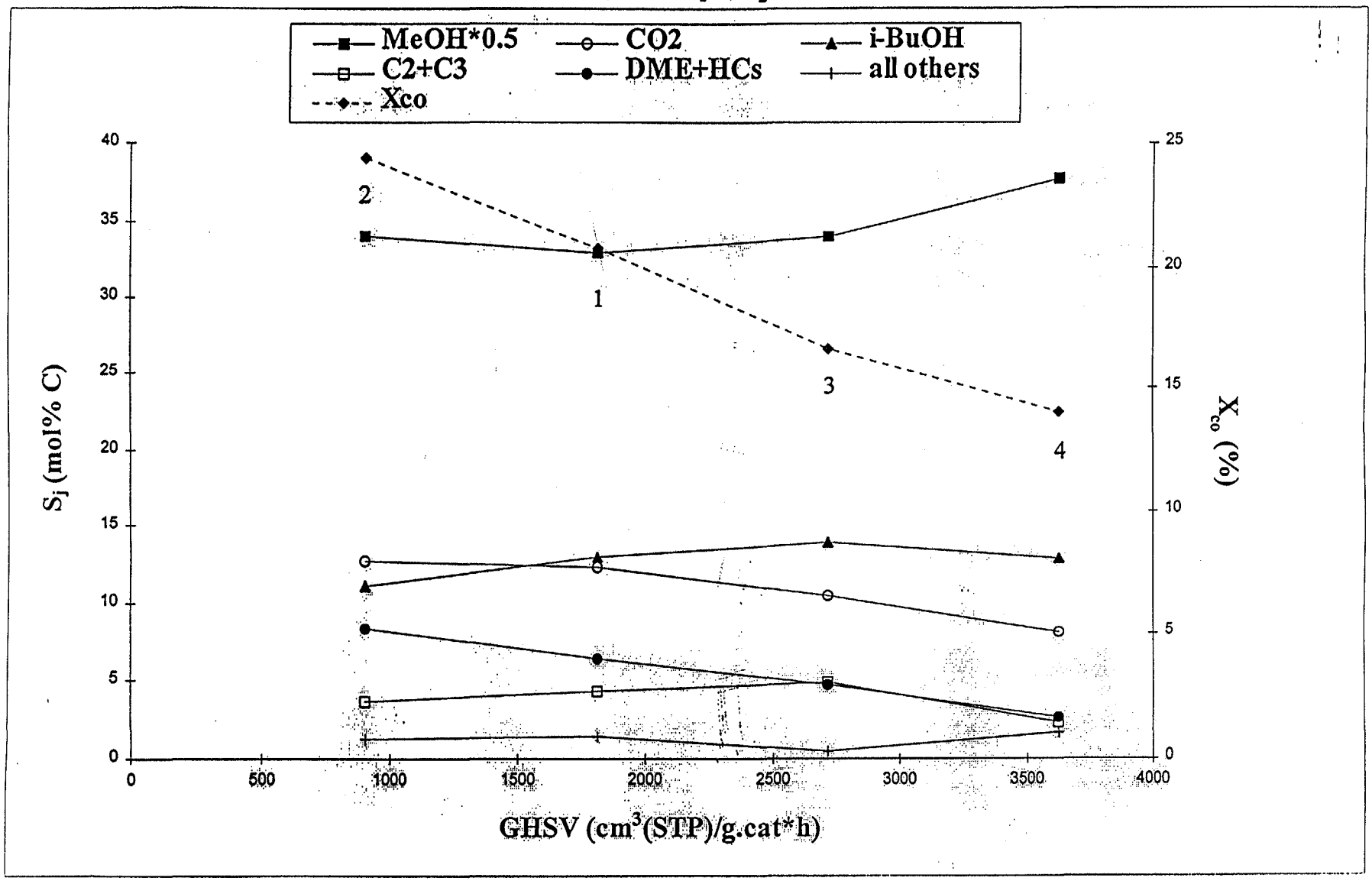

1,2,3,4 denote order in which experiment was performed

Fig. 18. **Product Selectivities vs. Space Velocity**

CMRU-13B: K-$Cu_{0.5}Mg_5CeO_x$ (MG3-10 O/K)

T = 331 °C, P = 750 psi, H_2/CO = 1

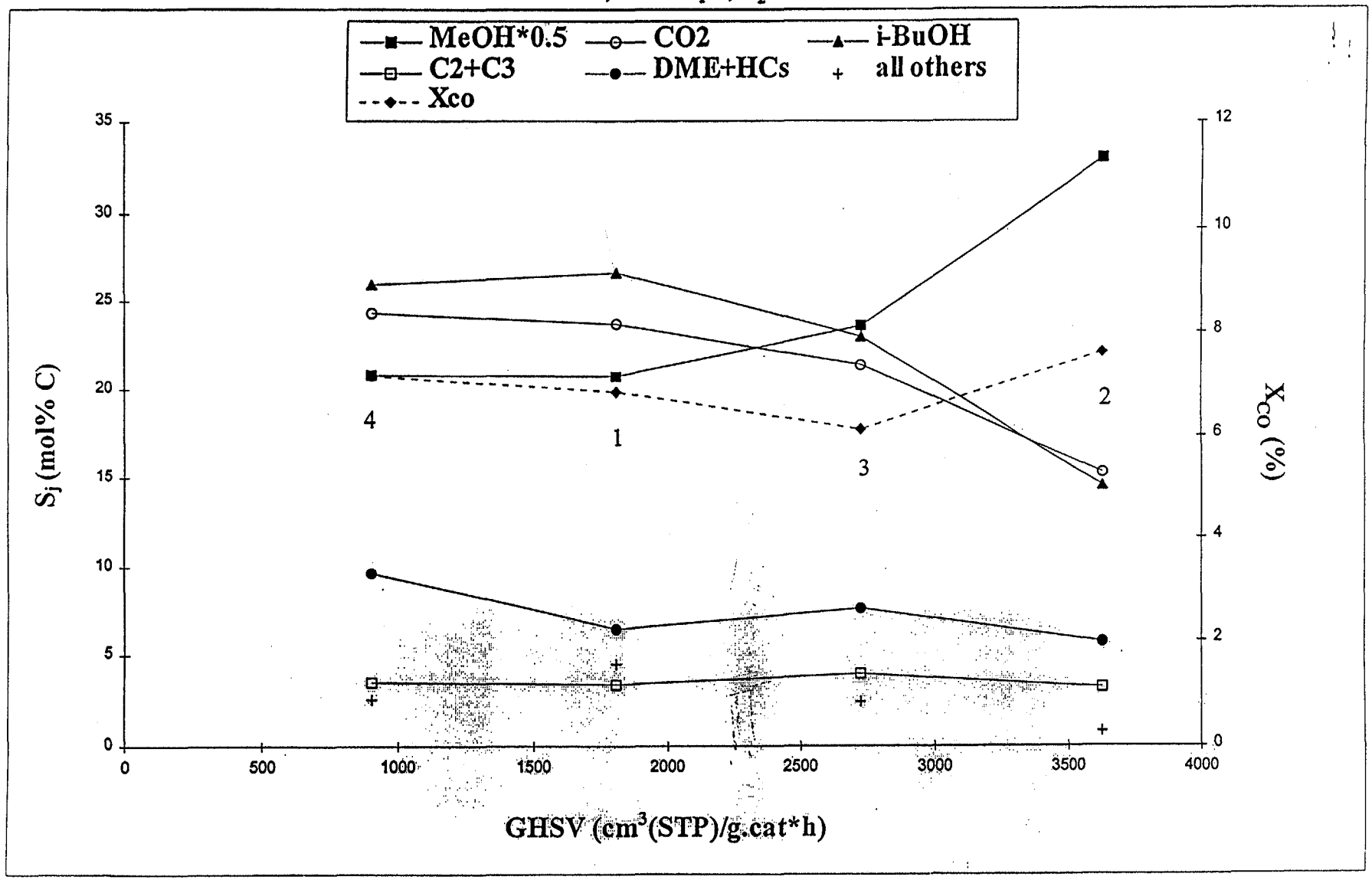

1,2,3,4 denote order in which experiment was performed

Fig. 19. Product Selectivities vs. Space Velocity

CMRU-14: $Cs\text{-}Cu_{0.5}Mg_5CeO_x$ (MG3-10 O/Cs)

T = 331 °C, P = 750 psi, $H_2/CO = 1$

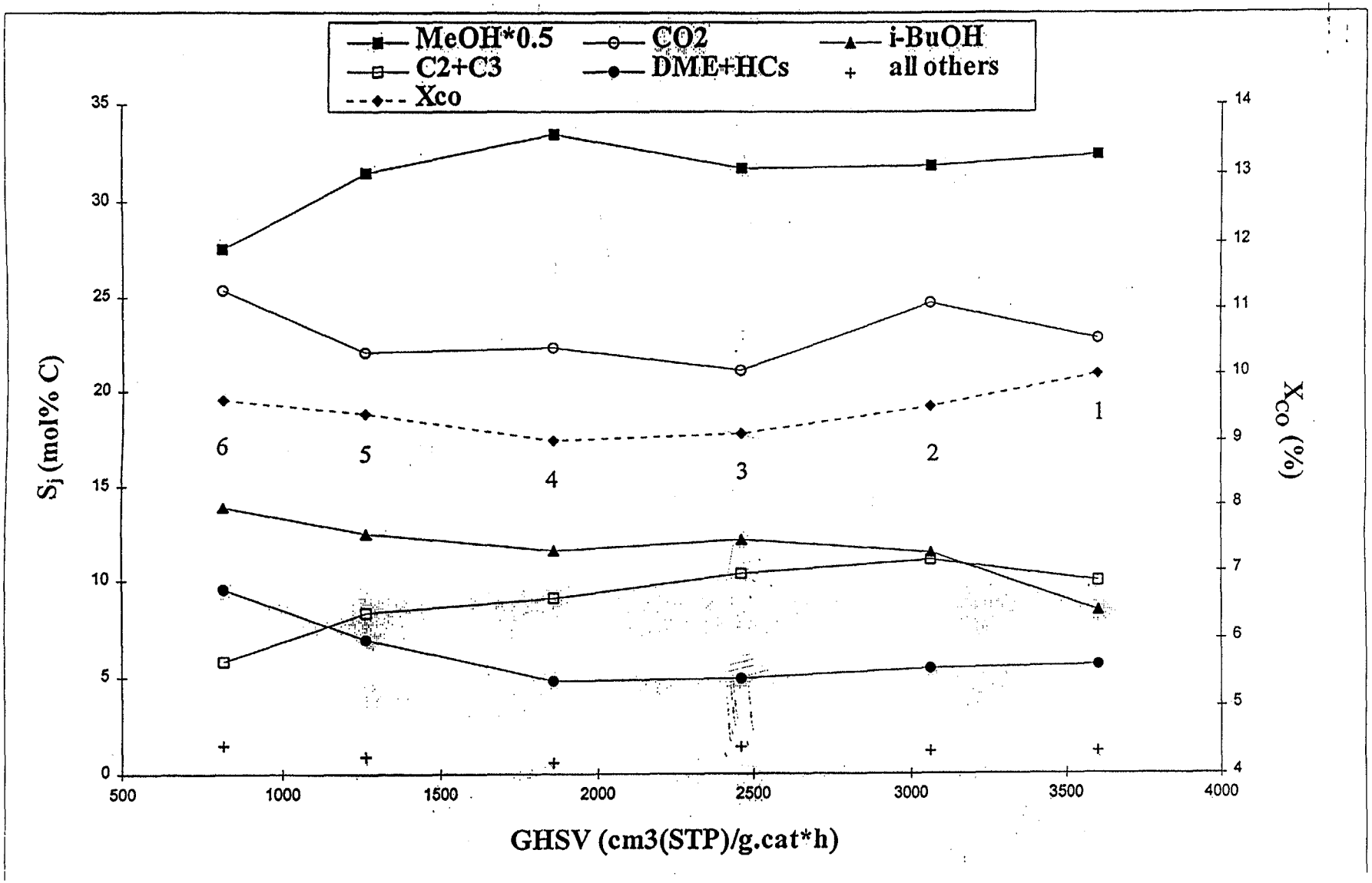

1,2,3,4,5,6 denote order in which experiment was performed

Fig. 20. Effect of CO_2 Pressure on Reaction Rate

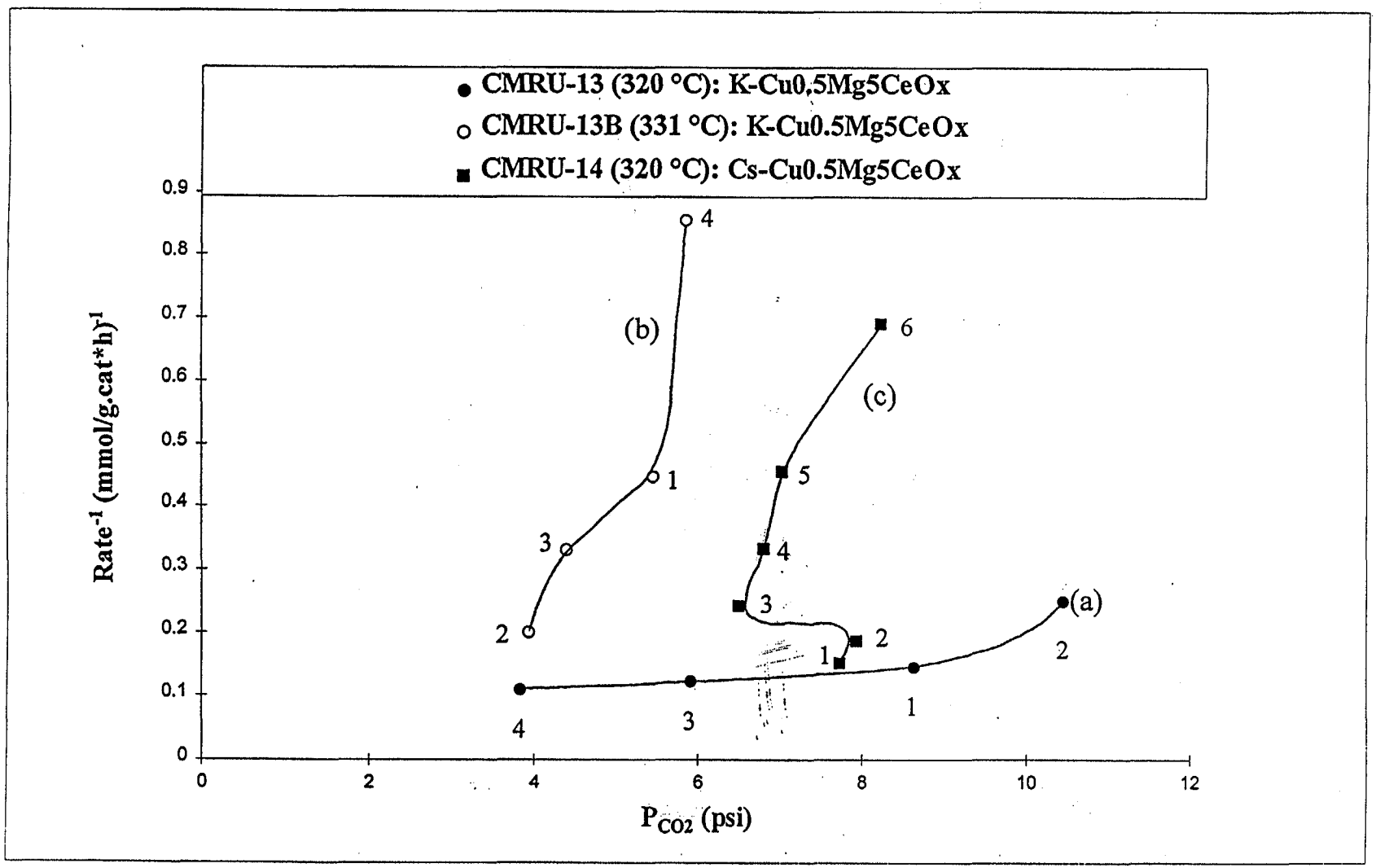

Numbers on plot denote order in which experiment was performed

Fig. 21 CH_3CHO TPSR

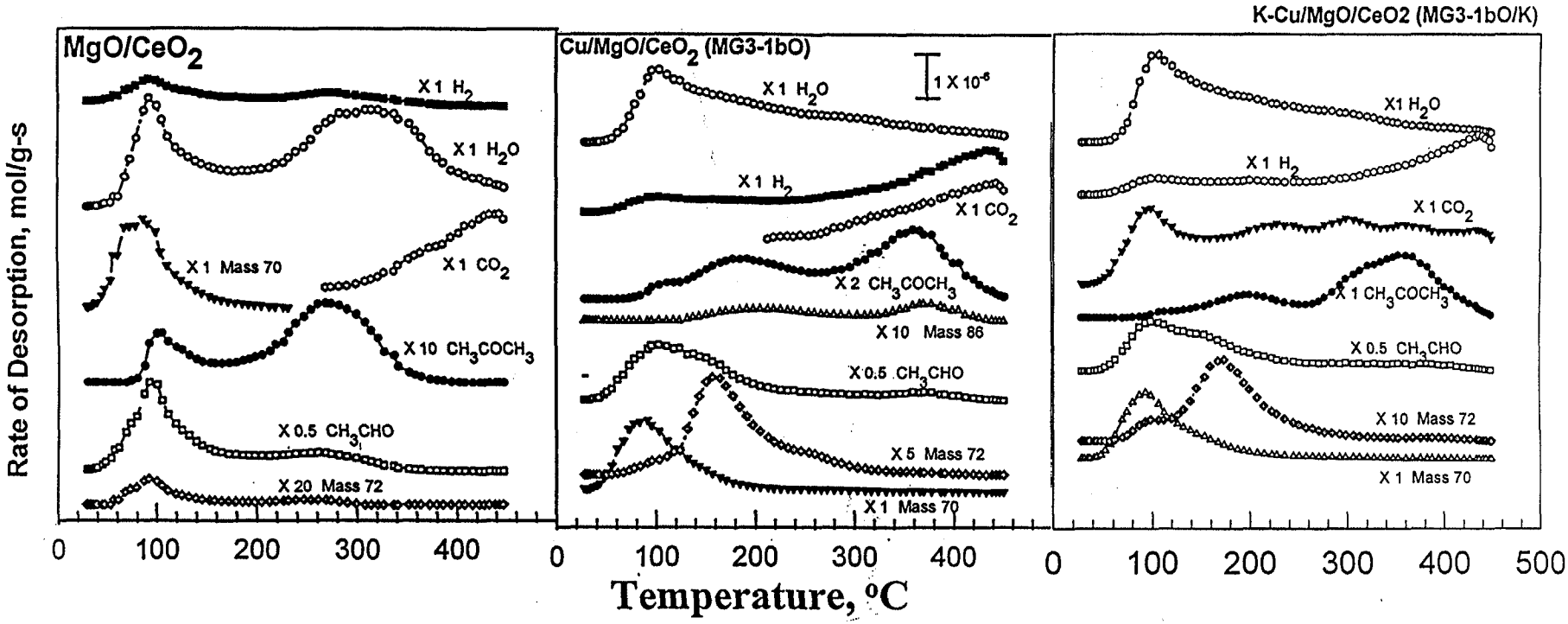

Fig. 22 Acetaldehyde TPSR on K-Cu/MgO/CeO_2

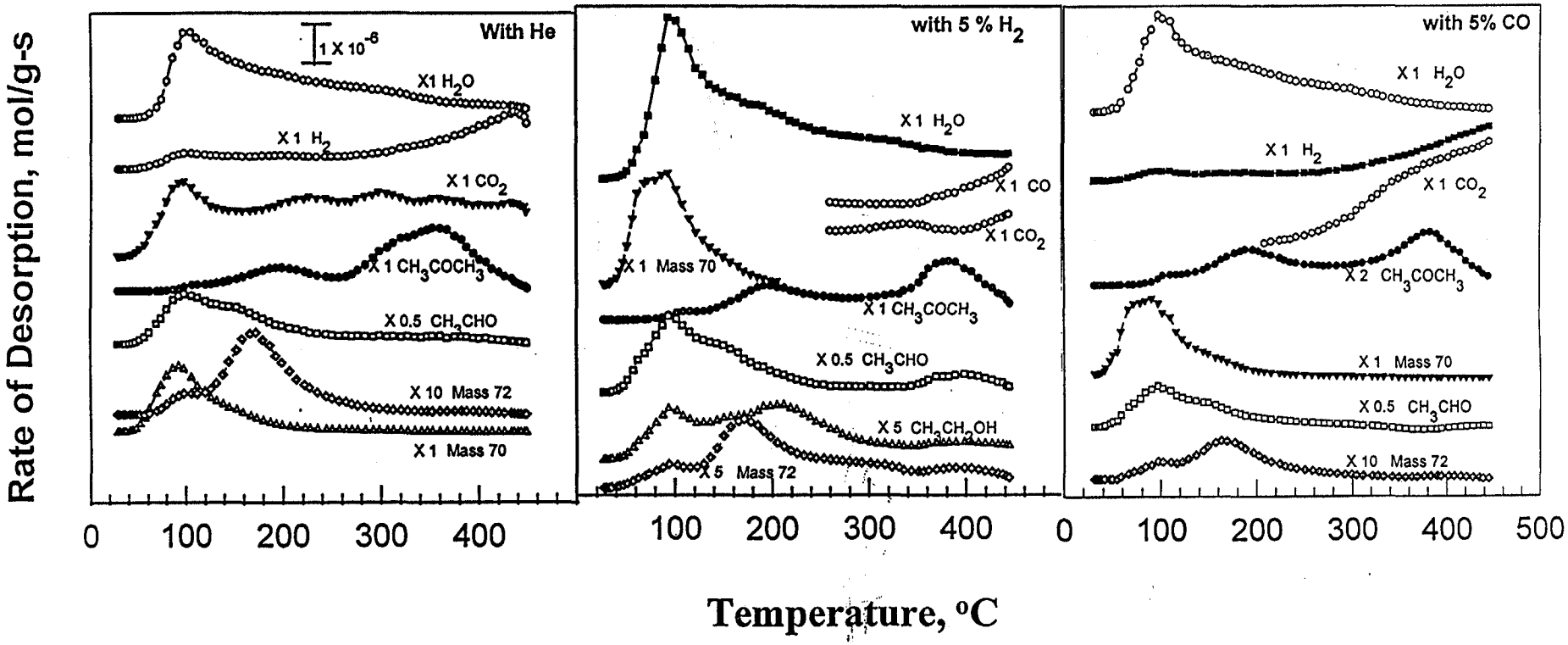

Fig.24 Ethanol TPSR

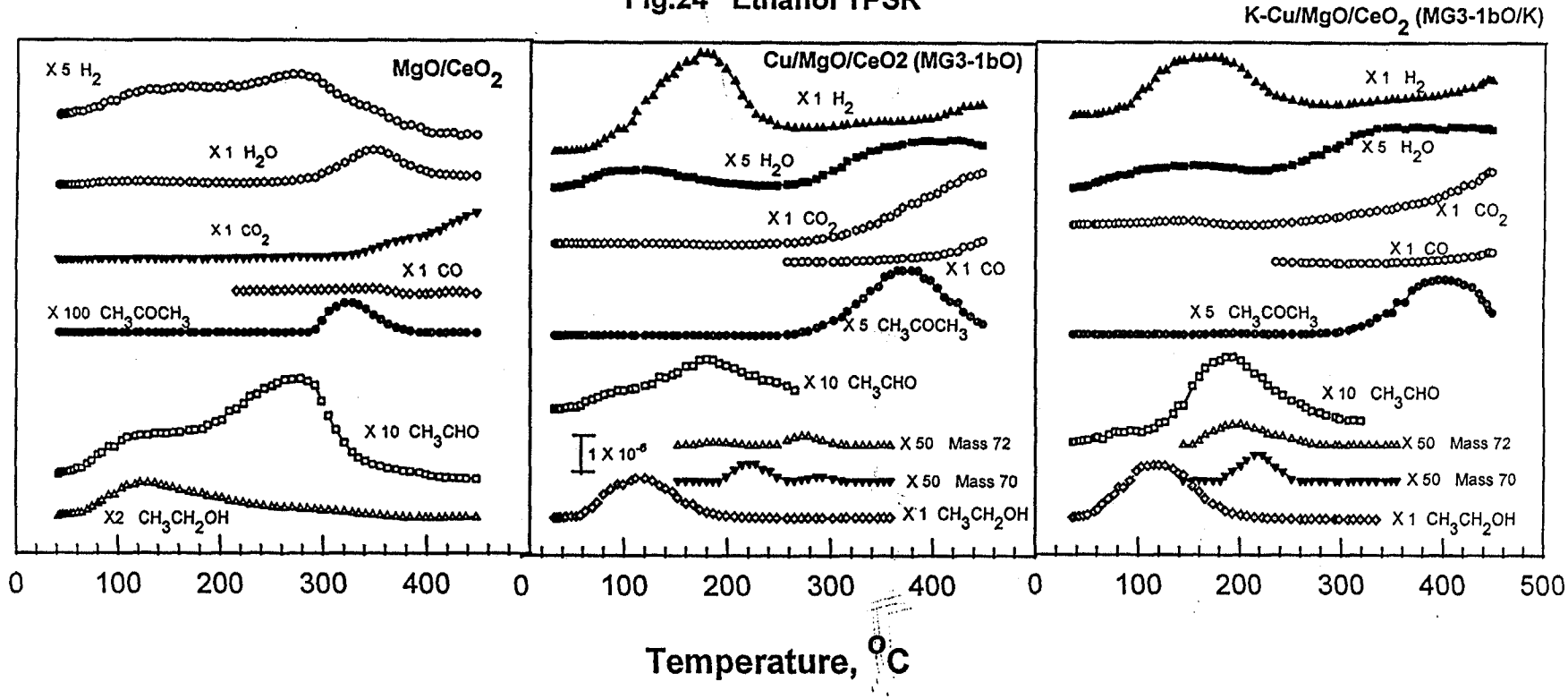

Fig. 25 Ethanol TPSR over Cu/MgO (MG3-5 O)

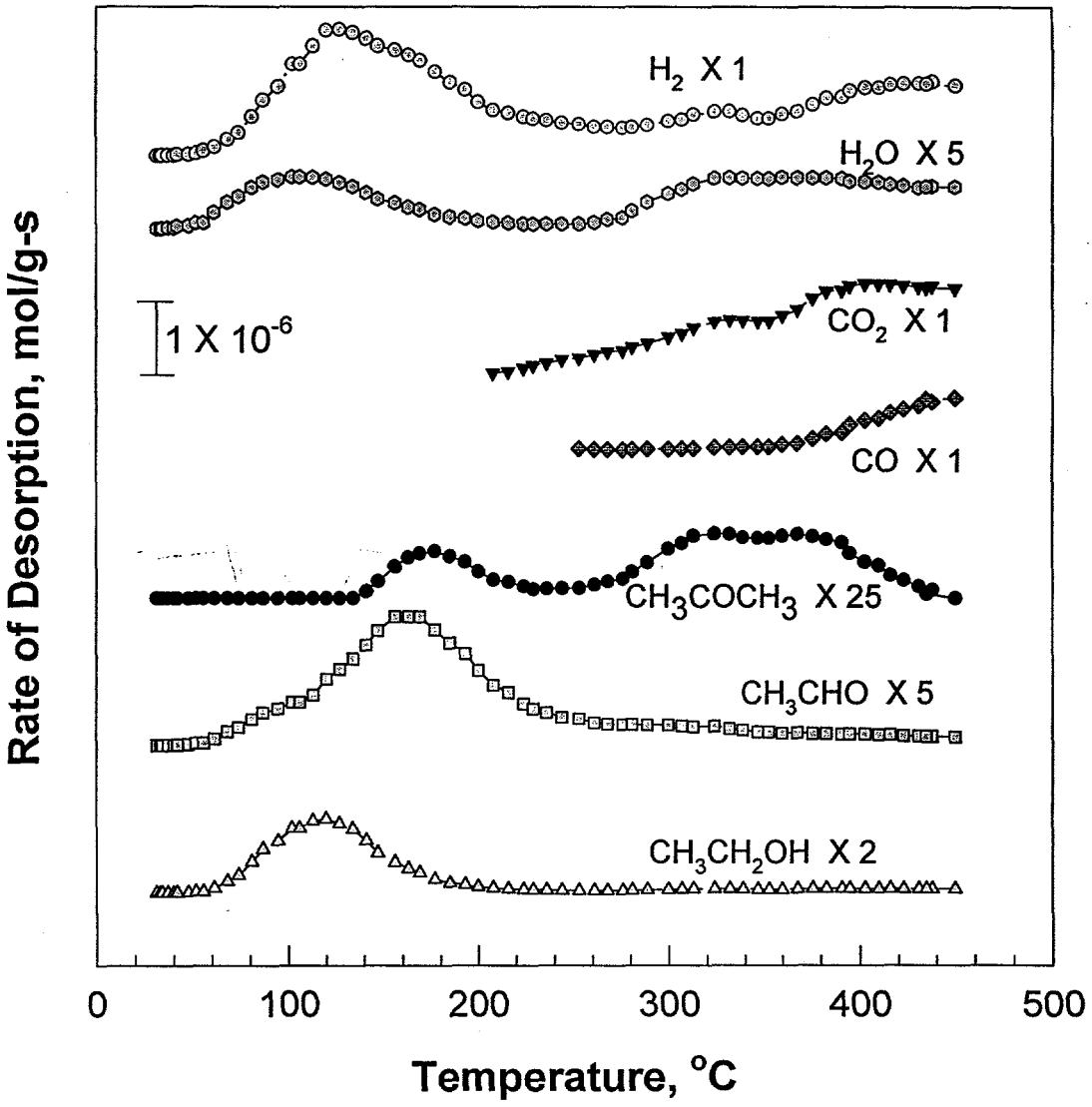

Fig.26 Ethanol TPSR over K-Cu/MgO/CeO_2 (MG3-1bO/K)

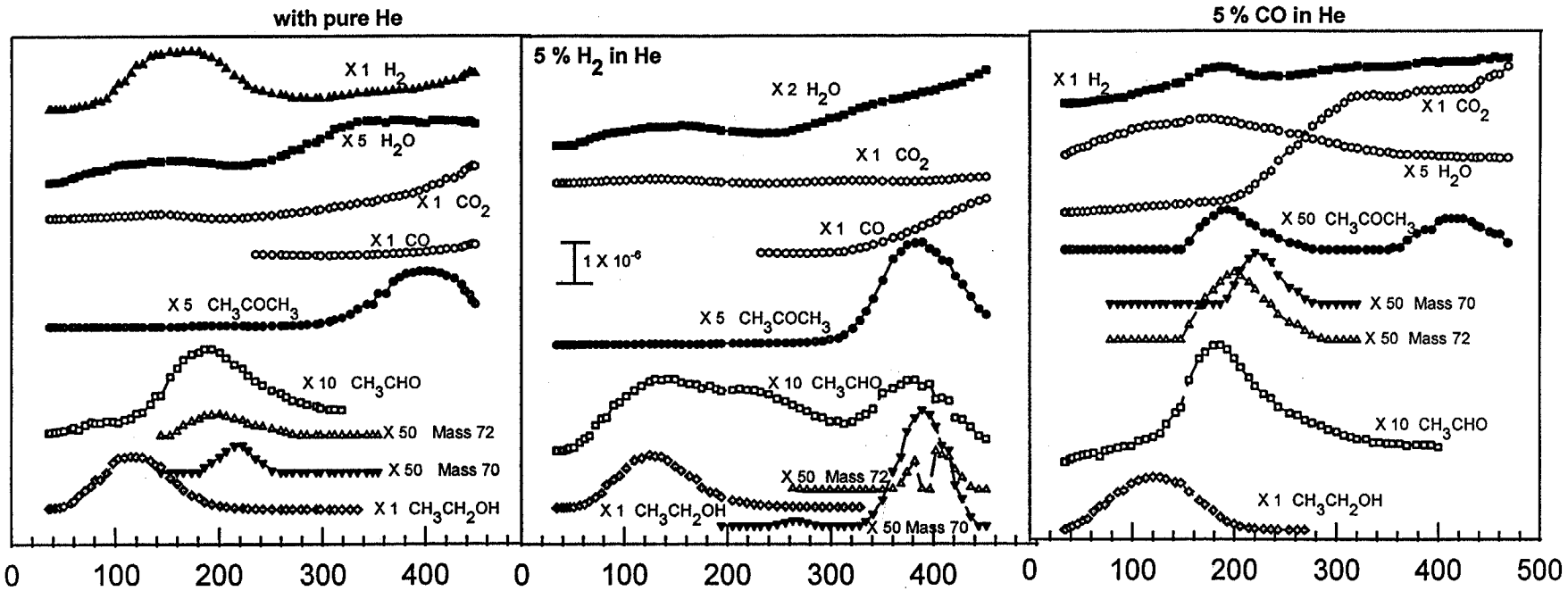

Fig. 27 CH_3OH TPSR

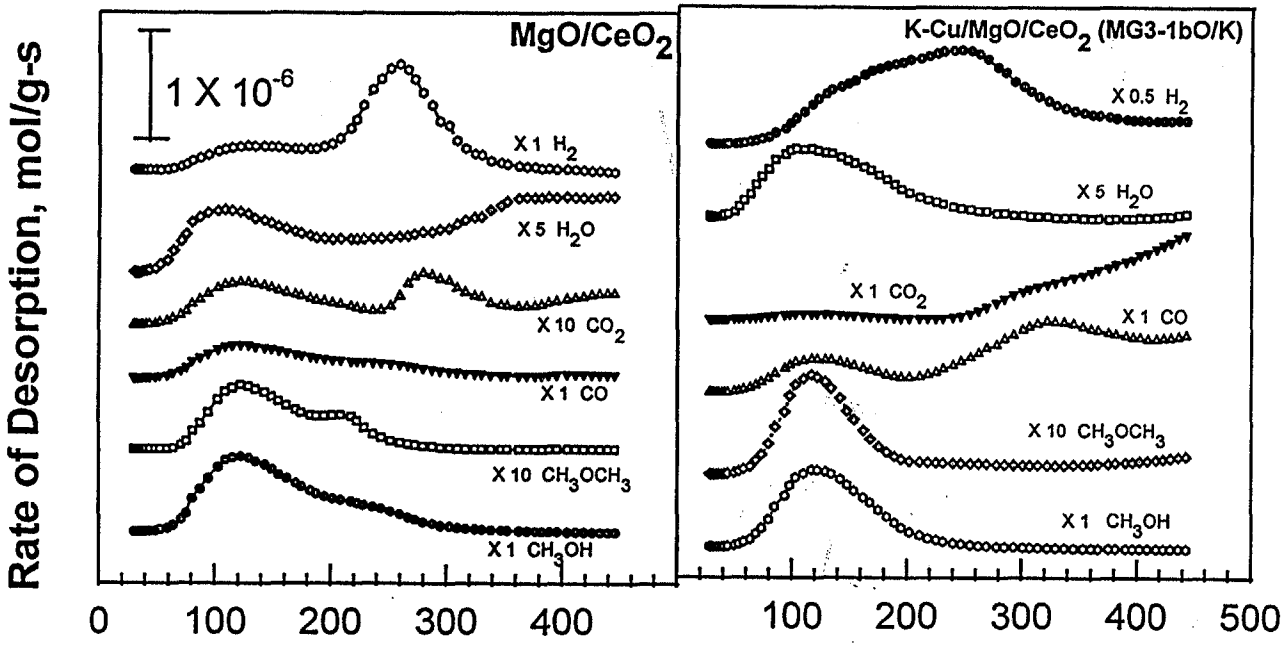

1. TITLE ISOBUTANOL- METHANOL MIXTURE FROM SYNGAS	2. REPORTING PERIOD Jan. 1, 1996 to Mar. 31, 1996	3. IDENTIFICATION NUMBER DE-AC22-PC94PC066
2. PARTICIPANT NAME AND ADDRESS Department of Chemical Engineering University of California- Berkeley, Berkeley, CA 94720	5. COST PLAN DATE Apr. 12, 1996	6. START DATE OCT 1994 7. COMPLETION DATE OCT 1997

8. Element code	9. Reporting element	ACCRUED COSTS				ESTIMATED ACCRUED COSTS							12. Total contract Value	13. Variance
		Reporting period		Cumulative to date		a.total this fiscal year	b. balance of fiscal year	c. FY96 (1)	d. FY 97 (2)	(3)		e. total		
		a. Actual	b. Plan	c. Actual	d. Plan									
	1. Total (Direct material)	18,949	22,777	59,853	119,597	35,060	56,049	91,109	94,782			210,684	259,929	49,245
	a) Purchased Parts	12,217	9,106	51,826	39,763	28,257	8,168	36,425	40,200			100,194	98,175	-2,019
	b) Subcontracted Items	2,114	13,670	2,114	79,833	2,114	52,565	54,679	54,582			109,261	161,754	52,493
	c) Other	4,618	0	5,913	0	4,689	0	0	0			5,913	0	-5,913
	2. Material Overhead	0	0	0	0	0	0	0	0			0	0	0
	3. Direct Labor 'Total	15,635	20,892	76,261	122,136	29,640	53,929	83,569	92,812			223,002	256,725	33,723
	4. Labor Overhead	0	0	0	0	0	0	0	0			0	0	0
	5. Fringe Benefits	1,828	3,350	8,966	19,468	3,641	9,759	13,400	15,368			34,093	41,538	7,445
	6. Special Testing	388	0	433	0	433	0	0	0			433	0	-433
	7. Special Equipment	15,402	2,000	285,980	256,000	41,802	-33,802	8,000	0			252,178	260,000	7,822
	8. Travel	2,426	1,629	5,882	9,463	3,694	2,821	6,515	7,020			15,723	19,740	4,017
	9. Consultants	0	0	0	0	0	0	0	0			0	0	0
	10. Other Direct costs	0	6,114	0	35,518	0	24,455	24,455	25,677			50,132	73,422	23,290
	11. Direct costs and Overhead	54,627	56,761	438,941	562,180	114,270	112,774	227,044	235,653			787,368	911,354	123,986
	12. General and Administrative Expense '49.5 %	19,573	20,505	76,215	124,747	36,162	45,858	82,020	90,358			212,430	256,108	43,678
	13. Facilities Capital Cost of Money	0	0	0	0	0	0	0	0			0	0	0
	14. Total Estimated Cost	74,200	77,266	515,157	686,926	150,432	158,630	309,062	326,008			999,795	1,167,462	167,667
	15. Fee	0	0	0	0	0	0	0	0			0	0	0
	16. Cost Sharing	9,786	9,949	204,163	232,953	15,408	24,389	39,797	56,789			285,341	301,651	16,310
	17. Total estimated DOE funds spent = Item 14-Item 16	64,414	67,316	310,994	453,974	135,024	134,241	269,265	269,219			714,454	865,811	151,357
14. Total		64,414	67,316	310,994	453,974	135,024	134,241	269,265	269,219			714,454	865,811	151,357

15. DOLLARS EXPRESSED IN	16. SIGNATURE OF PARTICIPANT PROJECT MANAGER AND DATE	17. SIGNATURE OF PARTICIPANT'S AUTHORIZED FINANCIAL SERVICE REPRESENTATIVE AND DATE
One U.S. Dollar		Lourdes J. Ferrer 4/12/96

DOE F 1332.3
(11-84)

U.S. DEPARTMENT OF ENERGY
MILESTONE SCHEDULE ☐ PLAN ☒ REPORT

FORM APPROVED
OMB 1901-1400

1. TITLE	2. REPORTING PERIOD	3. IDENTIFICATION NUMBER
ISOBUTANOL METHANOL MIXTURE FROM SYNGAS	Jan 1, 1996 - March 31, 1996	DE - AC22 - PC94PC066

4. PARTICIPANT NAME AND ADDRESS	5. START DATE	6. COMPLETION DATE
Department of Chemical Engineering University of California - Berkeley	Oct 1994	Sept 1997

7. ELEMENT CODE	8. REPORTING ELEMENT	9. DURATION	10. PERCENT COMPLETE a Plan	b Actual
		94 — 95 — 96 — 97 O N D Q2 Q3 Q4 O N D J F M A M J J A S Q1 Q2 Q3 Q4		
	Task 3	Complete design, construction and start-up of packed bed reactor module	100	100
	Task 2	Prepare Cu-based catalyst compositions and characterize structure, surface area, and effectiveness of several synthetic approaches	100	100
	Task 2	Choose four promising materials for catalyst evaluation	100	100
	Task 3	Construct recirculating reactor module Establish reaction pathways and rate-determining steps	100	100
	Tasks 2 & 3	Identify catalyst components necessary to catalyze rate-determing steps that have been determined	100	80
	Tasks 2 & 3	Identify synthetic techniques to increase the reactivity and accessibility of such required sites	100	80
	Task 4	Complete construction and start-up of temperature programmed surface reaction apparatus and design of high-pressure infrared cell	100	100
	Task 4	Design and construction of high-pressure infrared cell	100	70
	Task 4	Calibrate between UCB and APCI laboratories by testing two selected catalysts in slurry reactors	100	20
	Task 2	Determine the density and reactivity of the required sites and implement synthetic methods to improve them	25	25

DOE F 1332.3
(11-84)

U.S. DEPARTMENT OF ENERGY
MILESTONE SCHEDULE ☐ PLAN ☒ REPORT

FORM APPROVED
OMB 1901-1400

1. TITLE	2. REPORTING PERIOD	3. IDENTIFICATION NUMBER
ISOBUTANOL METHANOL MIXTURE FROM SYNGAS	Jan 1, 1996 - March 31, 1996	DE - AC22 - PC94PC066

4. PARTICIPANT NAME AND ADDRESS	5. START DATE	6. COMPLETION DATE
Department of Chemical Engineering University of California - Berkeley	Oct 1994	Sept 1997

7. ELEMENT CODE	8. REPORTING ELEMENT	9. DURATION	10. PERCENT COMPLETE a Plan	b Actual
		94: O N D Q2 Q3 Q4 · 95: O N D J F M A M J J A S Q1 Q2 Q3 Q4 · 96: Q1 Q2 Q3 Q4 · 97:		
	Task 4	Identify reaction intermediates by TPSR and high pressure infrared methods	20	20
	Tasks 3 & 5	Identify catalysts with highest isoalcohol yields (two) and evaluate at conditions resembling envisioned commercial practice.	20	15
	Task 5	Assess economic viability of these catalytic materials	0	0
	Task 5	Complete testing of at least two selected catalysts in slurry reactors.	0	0
	Tasks 3 & 5	Choose two materials for detailed studies of the reaction mechanism and of optimum synthetic protocols	0	0
	Tasks 3 & 5	Complete mechanistic studies on most promising materials	0	0
	Tasks 2 & 5	Develop synthetic procedures that can be carried out on a commercial scale Suggest a range of catalyst compositions for future study.	0	0
	Task 5	Complete testing of the two selected catalytic materials	0	0
	Task 5	Assess future research requirements, technical readiness and economic viability of the most promising approach	0	0
		Produce final report	0	0